AD NUMBER

AD864945

LIMITATION CHANGES

TO:

Approved for public release; distribution is unlimited.

FROM:

**Distribution authorized to U.S. Gov't. agencies and their contractors;
Administrative/Operational Use; JAN 1970. Other requests shall be referred to Rome Air Development Center, Griffiss AFB, NY 13440.**

AUTHORITY

RADC ltr 17 Sep 1971

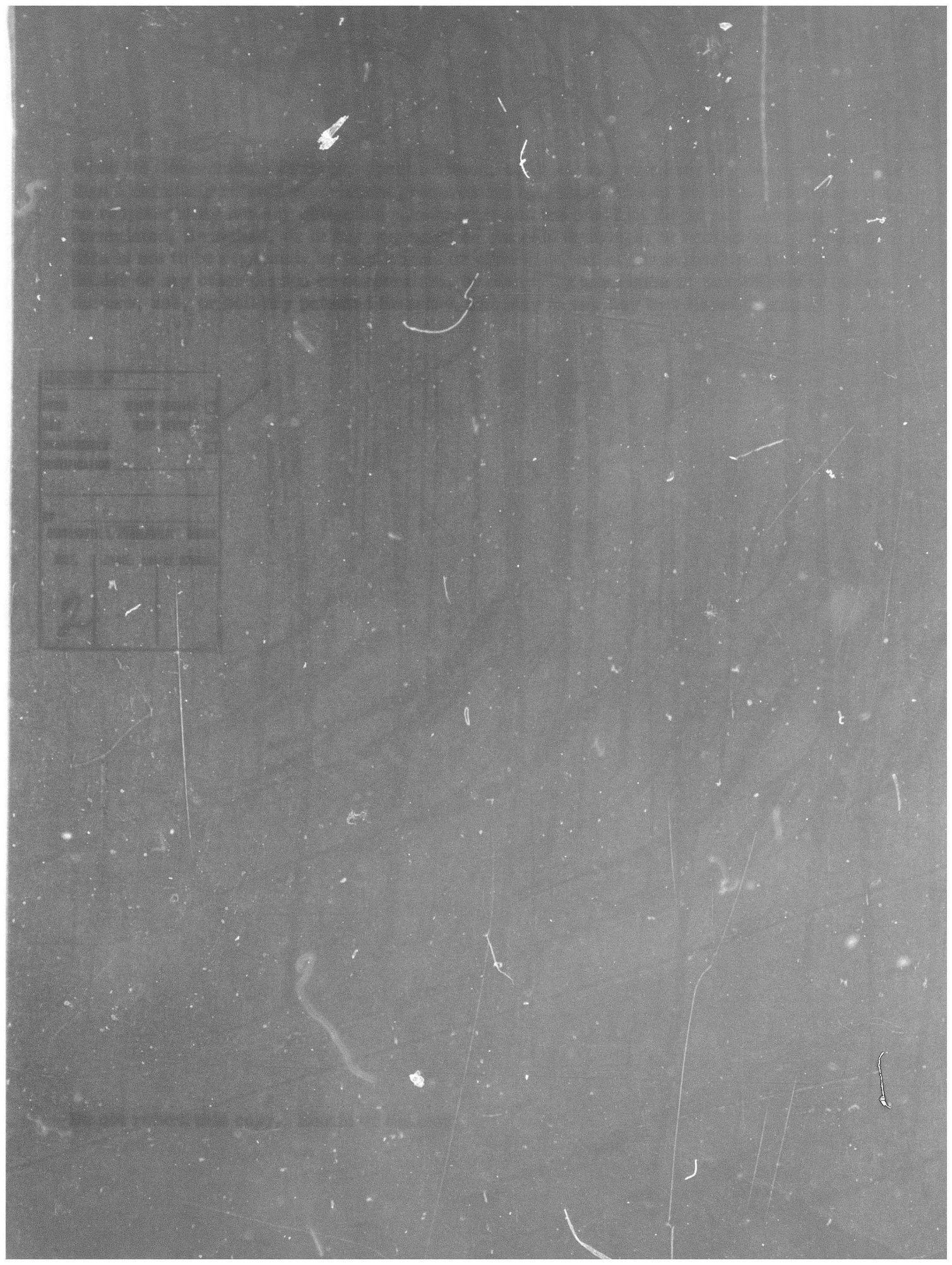

VARIABLE POLARIZER

L. J. Lovedan, Jr.

Sperry Microwave Electronics Division

FOREWORD

This Final Report covers the work performed on Contract No. F30602-68-C-0143, Project 4506, Task 450602 for the period December 1967 to November 1969. The submission date is November 1969.

The work on this contract is being performed by Sperry Microwave Electronics Division, Sperry Rand Corporation, Clearwater, Florida, 33717. It is under the direction of Mr. P. Romanelli (EMATE) of Rome Air Development Center, Griffiss Air Force Base, Rome, New York.

The secondary report number applied by Sperry Microwave to this report is SJ 219-5200-1.

Information in this report is embargoed under the U.S. Export Control Act of 1949, administered by the Department of Commerce. This report may be released by departments or agencies of the U.S. Government to departments or agencies of foreign governments with which the United States has defense treaty commitments. Private individuals or firms must comply with Department of Commerce export control regulations.

This technical report has been reviewed and is approved.

Approved: Patsy A. Romanelli
PATSY A. ROMANELLI
PROJECT ENGINEER
ELECTRON DEVICES SECTION

Approved:
LEO W. SULLIVAN
COLONEL, USAF
Chief, Surveillance & Control Division

FOR THE COMMANDER:
IRVING J. GABELMAN
Chief, Plans Office

ABSTRACT

The object of this work was to study and experimentally verify design criteria for a high power S band variable polarizer which transforms the TE_{10} mode to vertical linear, clockwise circular, counterclockwise circular, or horizontal linear polarizations. Design objectives include switching time less than 200 microseconds, and operation at 10 megawatts, 20 kilowatts average with a 40-microsecond pulse width, over the 3.1 to 3.6 GHz range. The polarizer is required to process both transmitted and receiver signals.

Nonreciprocal waveguide latching ferrite phase shifters (phasers) were studied as the active elements of the polarizer. A dual-channel configuration employing eight 90-degree phasers and a four-way power split were planned for the polarizer in order to minimize polarization errors and maximize yield of target signature information.

Breadboard phasers compatible with this concept were constructed on this program and tested for limiting, breakdown level, cooling effectiveness, and magnetostrictive effects.

These units employed boron nitride heat sinks along the vertical sides of the ferrite toroids, and a boron nitride toroid core in which cooling water was passed through a hollow stainless-steel charging wire. Ferrites with low normalized magnetizations were used to suppress limiting. The ferrite toroids were 12 inches long and produced about 40-degree phase shift with 0.5 to 1.0 dB loss.

The breadboard phasers showed no limiting up to 3 megawatts peak for normalized magnetizations as high as 0.383. Breakdown levels were above 3 megawatts peak for 2-microsecond pulse width, and 0.77 megawatt for 30-microsecond pulse width in units without charging wires at 25 psig air pressure. The units with charging wires broke down as low as 0.5 megawatt with a 2-microsecond pulse. Pressurization and the presence of hybrid mode "blips" in the transmission characteristics were found to have a significant influence on breakdown level.

Tests results indicated that waveguide height reduction would be needed to eliminate higher order mode resonances. This would probably make it necessary to split power more than four ways to achieve full power operation.

Program objectives were reduced to avoid the prohibitive expense of constructing full scale hardware.

TABLE OF CONTENTS

TABLE OF CONTENTS (Continued)

LIST OF ILLUSTRATIONS

SECTION I

INTRODUCTION

1.1 OBJECTIVE

The objective of this program is the study and experimental verification of criteria for the design of a high power S band variable polarizer. The function of the polarizer is to transform an input signal in the TE_{10} mode to vertical linear, clockwise circular, counterclockwise circular, and horizontal linear polarizations.

1.2 DESIGN GOALS

Frequency	3.1 to 3.6 GHz
Power	10 MW peak, 20 kW av
VSWR	1.2:1 max
Insertion loss	1 dB max at band edges
Switching time	200 μsec max
Pulse width	40 μsec min
Pulse repetition rate	70 pps nominal
Isolation between polarization channels	30 dB min
Phase nonlinearity at each polarization	$\leq \pm 2.5^{\circ}$ combined peak and random rms
Phase nonlinearity excluding that due to the waveguide	5° max
Amplitude response	0.5 dB combined peak and random rms

Differential phase and amplitude between polarization channels

Phase	0.5° max
Amplitude	0.2 dB max

Drift

Phase	1°/hr max
Amplitude	0.2 dB/hr max

Environmental temperature

Operating	-22°C (-10°F) to +49°C (120°F)
Nonoperating	-40°C (-40°F) to +49°C (120°F)

1.3 APPROACH

The system application required that the polarizer feed two equal amplitude outputs to the orthogonal arms of an orthomode transducer in the system. The orthogonal arms of the transducer would be oriented 45 degrees off vertical so the orthogonal components would combine in the transducer to form a resultant output in circular or square waveguide, with spatial polarization determined by the time phase relationships of the orthogonal inputs. (See Figure 1.)

Linear Vertical Output	A $\angle 0^\circ$		B $\angle 0^\circ$
Circular Right-hand Output	A $\angle 0^\circ$		B $\angle +90^\circ$
Circular Left-hand Output	A $\angle +90^\circ$		B $\angle 0^\circ$
Linear Horizontal Output	A $\angle 180^\circ$		B $\angle 0^\circ$

Vector directions represent spatial relationships. Angular notations represent time phase of input components.

Figure 1. Typical Input and Output Phase Relationships at the Orthomode Transducer

The polarizer design concept involves use of ferrite latching differential phase shifters (Figure 2) to set up the required phase relationships in two equal amplitude signals fed to the transducer. A waveguide hybrid divides the transmitted signal into two separate polarizer channels. Additional hybrids further divide and recombine these signals so each individual phaser carries one-fourth of the total power.

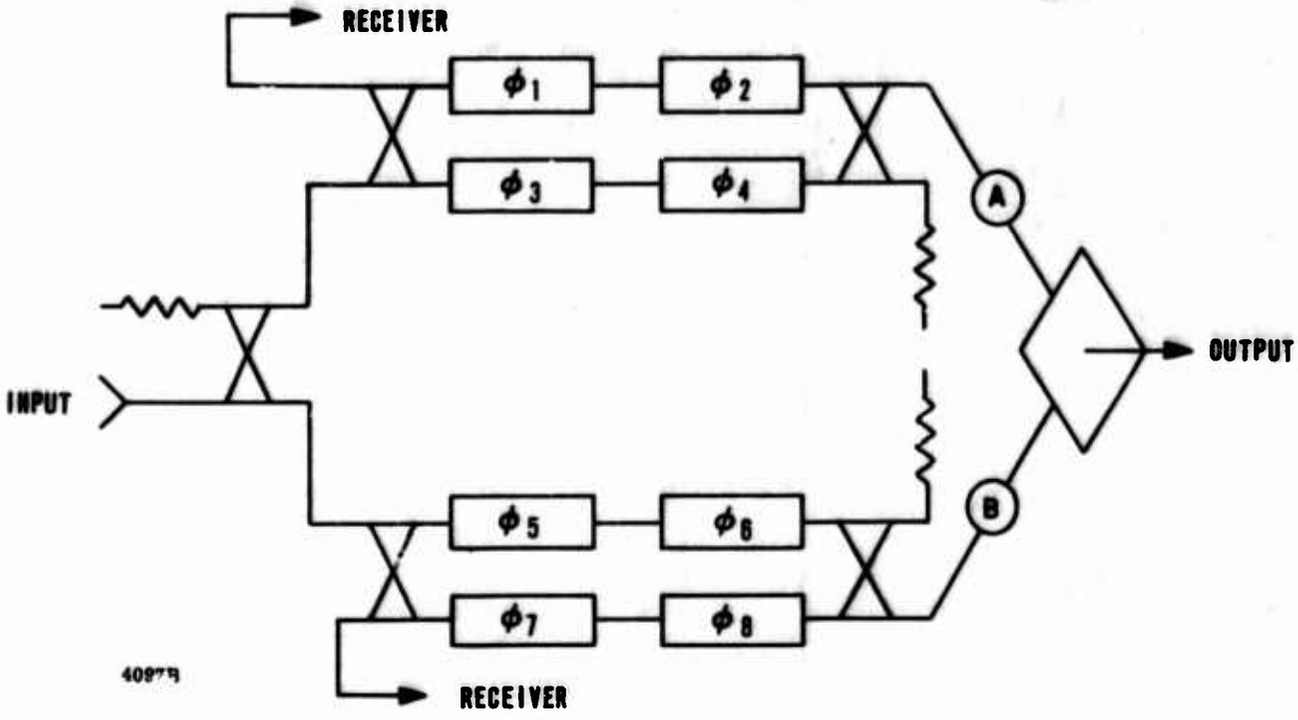

Figure 2. Dual-channel Receiver Polarizer

The phase shifters are nonreciprocal and provide a duplexing action which retains phase and amplitude information for the separate orthogonal components and permits reduction of target signature information from received signals scattered into various polarizations.

Combinations of phase relationships required to set up the various polarization conditions are shown in Table I.

The ultimate physical arrangement of the polarizer was conceived as resembling Figure 3.

Table I. Phase Shift of Each Element for Various Polarizations

Polarization	PHASER POSITION ϕ_1	ϕ_2	ϕ_3	ϕ_4	ϕ_5	ϕ_6	ϕ_7	ϕ_8
TRANSMIT CONDITION								
→	0	0	0	0	0	0	0	0
←	-90	-90	-90	-90	-90	-90	-90	-90
↑	-90	-90	-90	-90	0	0	0	0
↓	0	0	0	0	-90	-90	-90	-90
↷	0	-90	0	-90	0	0	0	0
	-90	0	-90	0	0	0	0	0
	-90	-90	-90	-90	-90	0	-90	0
	-90	-90	-90	-90	0	-90	0	-90
↶	0	0	0	0	-90	0	-90	0
	0	0	0	0	0	-90	0	-90
	0	-90	0	-90	-90	-90	-90	-90
	-90	0	-90	0	-90	-90	-90	-90
RECEIVE CONDITION								
Any Polarization	-90	-90	0	0	0	0	-90	-90
	0	0	-90	-90	0	0	-90	-90
	-90	-90	0	0	-90	-90	0	0
	0	0	-90	-90	-90	-90	0	0

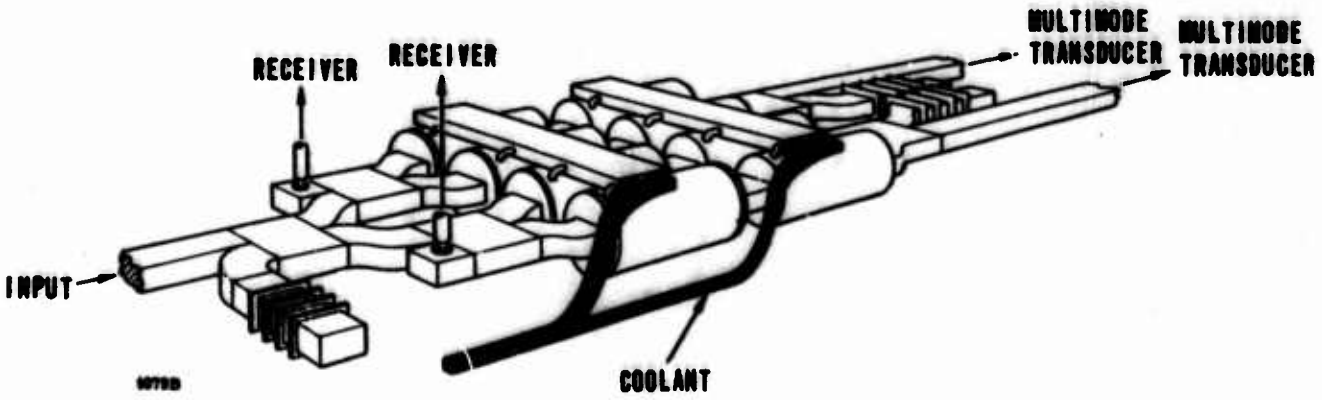

Figure 3. Dual-receiver Output Polarizer - Preliminary Layout

SECTION II

SUMMARY OF PRIOR WORK ON CONTRACT F30602-67-C0004

2.1 GENERAL

The prior contract[1] was a study of the basic latching polarizer problem. An analysis was made of factors affecting the polarization ellipse, and of the basic latching phase shifter design. The phaser cross section of Figure 4, employing boron nitride heat sinks and a water-cooled toroid core, was tentatively selected on the basis of this work.

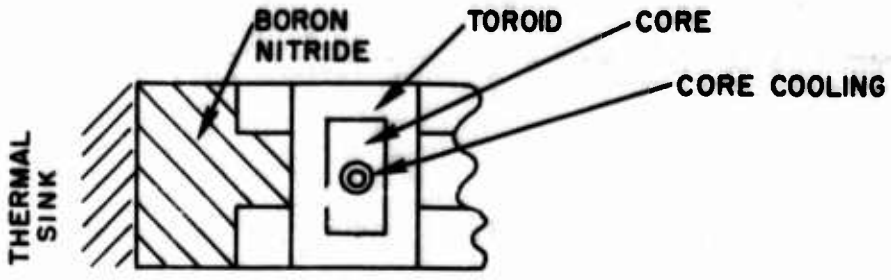

Figure 4. Phaser Cross Section

2.2 CONFIGURATION SELECTION

To minimize differences in rf heating between the various phasers used in the polarizer, the individual phasers should all operate at the same power level. The single-channel receiver shown in Figure 5 and the dual-channel configuration of Figure 2 both satisfy this requirement. These were analyzed and compared on the previous program. However, because the single-channel system does not accept received signals scattered into polarizations other than the transmitted signal, the dual-channel configuration was tentatively selected as superior. The latter system retains phase and amplitude information from the orthogonal components of the received signal. Further, the four-way power split which occurs naturally in the latter system results in proportionately lower power to the individual phasers.

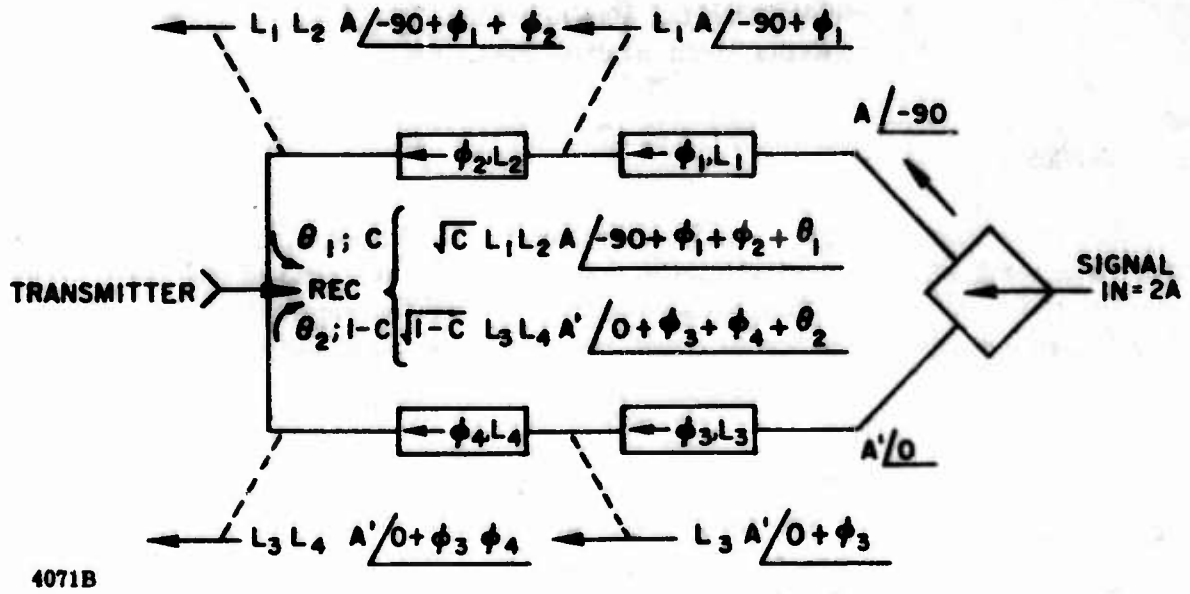

Figure 5. Signal Relationships in Single-receiver Port Polarizer

2.3 EXTERNAL SIGNAL POLARIZATION ANALYSIS

A study was made of the effects of phase and/or amplitude errors in signals reaching the orthomode transducer on the polarization of the transmitted signal. This study dealt with the following specific types of errors:

Case I: Polarization tilt in a linear polarized signal, caused by $C \neq D$ and/or $\theta_x - \theta_y \neq 0$ (Figure 6a);

Case II: Unwanted ellipticity in a linear polarized signal, caused by $C = D$ and $\theta_x = \theta_y \neq 0$ (Figure 6b);

Case III: Unwanted ellipticity with tilted major axis in a circular polarized signal, caused by $C \neq D$; $\left|\theta_x - \theta_y\right| = 90^o$ (Figure 6c), or

Case IV: Unwanted ellipticity without a tilted major axis in a circular polarized signal where C = D ; $|\theta_x - \theta_y| \neq 90^o$ (as in Figure 6c but with the major axis along either the horizontal or vertical direction).

Error magnitudes associated with -30 dB unwanted signal components were determined to be as follows:

Table II

Case	Input	Allowable Error	
		θ_x, θ_y Phase (Degrees)	C/D Amplitude (dB)
I	Linear	---	0.549
II	Linear	3^o 38'	---
III	Circular	---	0.2794
IV	Circular	1^o 50'	---

Operation in the circular polarized modes (Cases III and IV) is seen to be about twice as sensitive to errors as the linear polarized modes. The tabulated values provide an indication of the channel-to-channel differential phase and amplitude accuracy requirements which would be tolerable in a practical situation.

A detailed analysis of the properties of the polarization ellipse is given in Appendix I of this report.

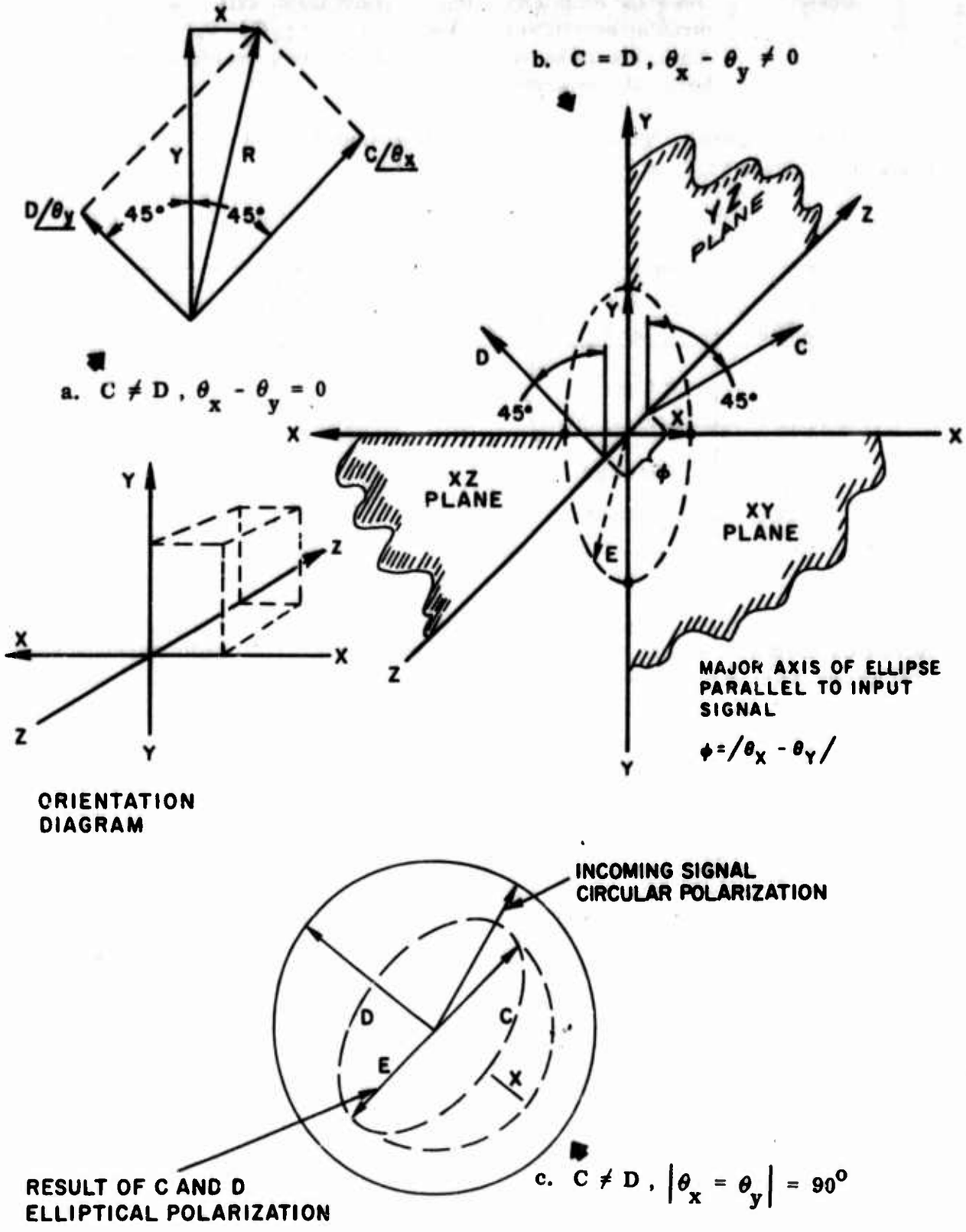

Figure 6. Error Resultant of Conditions

2.4 INTERNAL SIGNAL ERROR ANALYSIS

A computer study was also made to determine the effects of internal phase and coupling errors on the phase and amplitude of the polarizer outputs to the transducer. The circuit signal flow model and notation employed are shown in Figure 7.

In this analysis, a perfect initial power split is assumed (A = B = 1). Errors were introduced symmetrically in each channel as phase errors in the hybrids or phasers, or as coupling errors in the hybrids.

The applicable equations are as follows:

$$C = X_1^2 + X_2^2 + 2X_1X_2 \left(\cos \left[\delta_1 - \delta_2\right]\right)$$

$$\theta_x = \tan^{-1}\left[\frac{X_1 \sin \delta_1 + X_2 \sin \delta_2}{X_1 \cos \delta_1 + X_2 \cos \delta_2}\right]$$

$$D = Y_1^2 + Y_2^2 + 2Y_1Y_2 \left(\cos \left[\delta_3 - \delta_4\right]\right)$$

$$\theta_y = \tan^{-1}\left[\frac{X_1 \sin \delta_3 + Y_2 \sin \delta_4}{Y_1 \cos \delta_3 + Y_2 \cos \delta_4}\right]$$

where

$$X_1 = L_1L_3\sqrt{K_1}\sqrt{K_2}\sqrt{A}$$

$$X_2 = L_2L_4\sqrt{1-K_1}\sqrt{1-K_2}\sqrt{A}$$

$$Y_1 = L_5L_7\sqrt{L_3}\sqrt{K_4}\sqrt{B}$$

$$Y_2 = L_6L_8\sqrt{1-K_3}\sqrt{1-K_4}\sqrt{B}$$

$$\delta_1 = \theta_1 + \theta_2 + \phi_1 + \phi_3$$

$$\delta_2 = \phi_2 + \phi_4$$

$$\delta_3 = \theta_3 + \theta_4 + \phi_5 + \phi_7$$

$$\delta_4 = \phi_6 + \phi_8$$

The preceding terms are located in the diagram of Figure 7 and are defined as follows:

L terms - losses associated with phase shift elements

K terms - coupling factors of hybrids

A and B terms - output powers from multimode transducer

θ terms - phase shift through hybrids

φ terms - phase shift through phaser elements

Table III

Run*	Coupling Error	Phase Error		Output to Transducer		
					Angular Error	
	C=3 ±( ) dB	ϕ1-4	θ	A/C=B/D	θ_A	θ_B
1	0	ϕ_{5-6}^{1-2} ±5°	±5° max	.133 dB max	±0° 1.45'	±0° 1.45'
2	0	±2° max	±2° max	0	±4°	±4°
3	0	±5°	0	.033 dB	±4° 59.28'	±4° 59.28'
4	0	0	±5°	.033 dB	±5° 0.72'	±5° 0.72'
5	-0.1	0	±5°	.033 dB max	±5° 7.71'	±5° 7.71'
6	+0.1	0	±5°	.033 dB max	±4° 53.84'	±4° 53.84'

* 1 Phase slope of couplers adds to phase slope of phasers

2 Phase slope of coupler compensates for phase slope of phasers

3 Phase slope of phasers = 0

4 Phase slope of couplers = 0

5 Coupling -0.1 dB; coupling phase varied ±5°

6 Coupling +0.1 dB; coupling phase varied ±5°

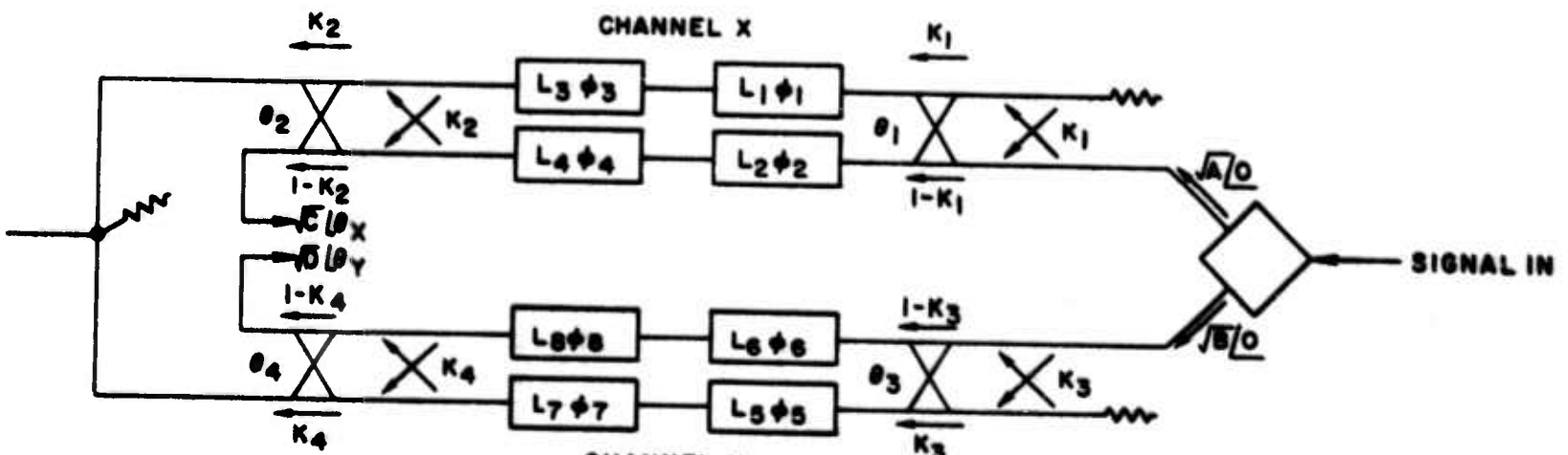

$$L_1 L_3 \sqrt{A}\sqrt{K}\,/\theta_1+\phi_1+\phi_3$$

$$L_1 \sqrt{A}\sqrt{K}\,/\theta_1+\phi_1 \qquad \sqrt{A}\sqrt{K}\,/\theta_1$$

$$L_1 L_3 \sqrt{K_1}\sqrt{K_2}\sqrt{A}\,/\theta_1+\theta_2+\phi_1\phi_3 = X_1/\delta_1$$

$$L_2 L_4 \sqrt{1-K_1}\sqrt{1-K_2}\sqrt{A}\,/\phi_2+\phi_4 = X_2/\delta_2$$

$$L_2 \sqrt{A}\sqrt{1-K_1}\,/0+\phi_3 \qquad \sqrt{A}/0$$

$$\sqrt{A L_2 L_4}\sqrt{1-K_1}\,/\phi_2+\phi_4 \qquad \sqrt{A}\sqrt{1-K}/0$$

40128-R

$$C = X_1^2 + X_2^2 + 2X_1X_2(\cos[\delta_1-\delta_2]);\ \theta_X = \tan^{-1}\left[\frac{X_1 \sin\delta_1 + X_2 \sin\delta_2}{X_1\cos\delta_1 + X_2\cos\delta_2}\right]$$

Figure 7. Dual-channel Receiver Balanced Polarizer with Signal Flow

Because of anticipated ability to balance channel-to-channel phase offset by length adjustment or IF phase adjustment, effects of channel asymmetry were not analyzed, nor were the effects of variations in L (loss). However, on the basis of computed data and anticipated system adjustment capability, C-D unbalance of 0.3 dB and $\theta_A - \theta_B$ values near 3 degrees were estimated to be realistic. Use might be made of complementary characteristics in the phasers and couplers to further improve balance or flatness.

The orthomode transducer was assumed perfect in the above analysis. Any phase and/or amplitude errors anticipated in the transducer would also have to be taken into account in an overall system error budget.

2.5 PHASER STUDIES

2.5.1 General

The configuration study had indicated the polarizer phaser should resemble Figure 2, employing a 4-way power split and eight identical 90-degree building block phasers feeding an orthomode transducer tilted 45 degrees. Each phaser would transmit one-fourth of the total transmitted power. This design permits all phasers to operate at the same power level and temperature.

The phaser cross section of Figure 8 was recommended for study on the present program, based on heat-dissipating capability and the need to minimize the chance of limiting and breakdown.

2.5.2 Heat Dissipation

Based on 5 kW average transmitted power and 0.5 dB loss per 90-degree element, approximately 500 watts could be dissipated in each toroid. In order to avoid magnetostrictive effects, it was deemed necessary to maintain a thermal stress level well below 500 psi. Figures 9 and 10 summarize the findings of the prior program regarding approximate dimensional relationships required to maintain given stress levels at 500 watts dissipated. Ferrite is assumed to have a thermal resistance of 6.7°C/W/in.^{2}/in., and a modulus of elasticity of approximately 25×10^6. Stress is assumed to be bending stress resulting from the temperature differential through the toroid wall with the toroid wall constrained flat. Core cooling was considered essential, since it reduces temperature differential to about one-quarter of what it would be with external cooling only, as shown in Figures 8 and 9.

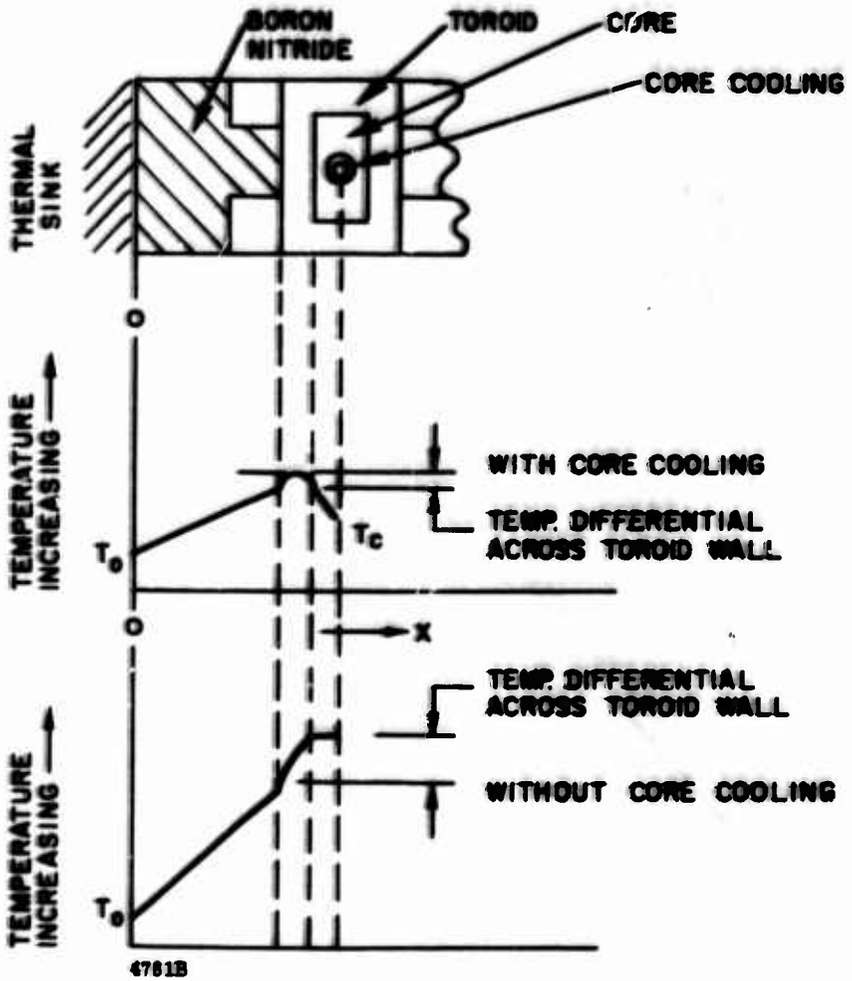

Figure 8. Temperature Gradient of Phase Shifter Cross Section With and Without Core Cooling

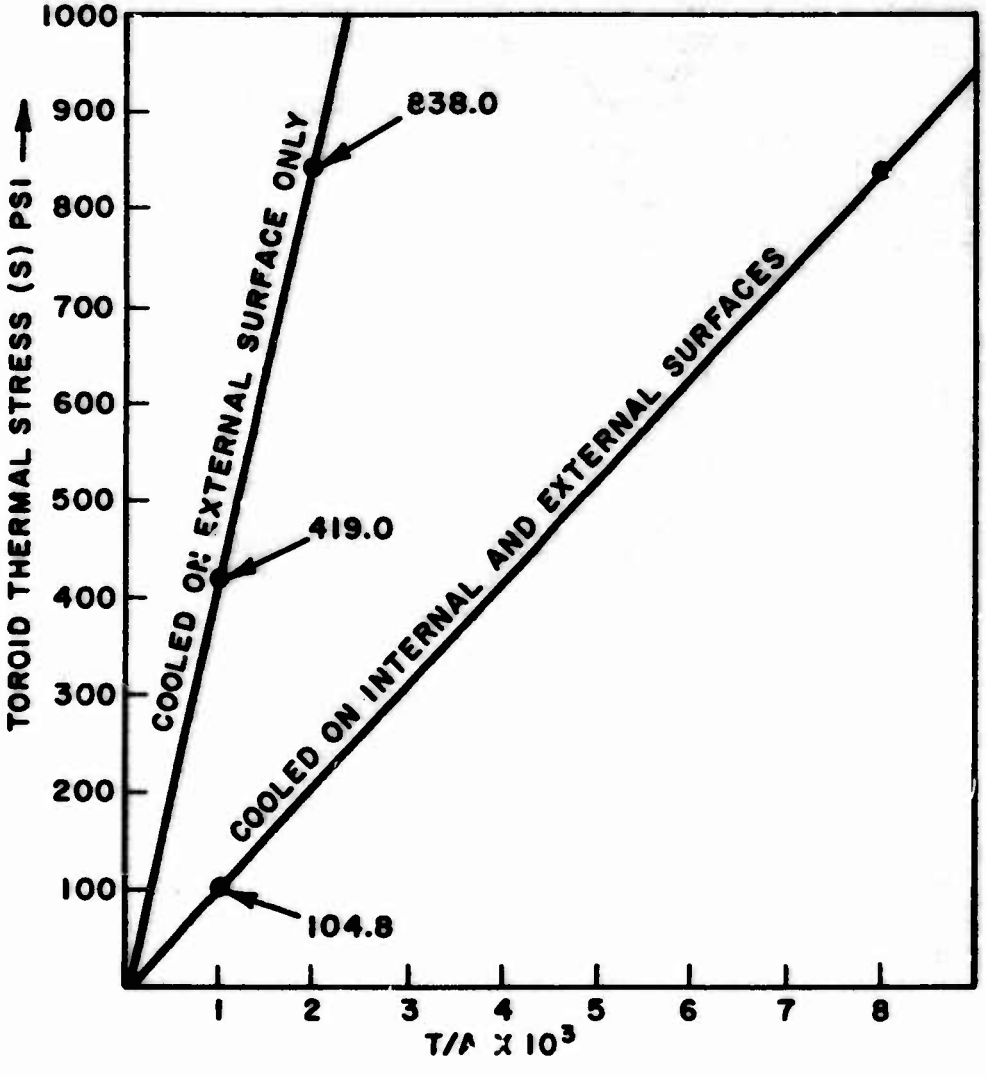

Figure 9. Toroid Thickness to Area Ratio for Two Cooling Approaches

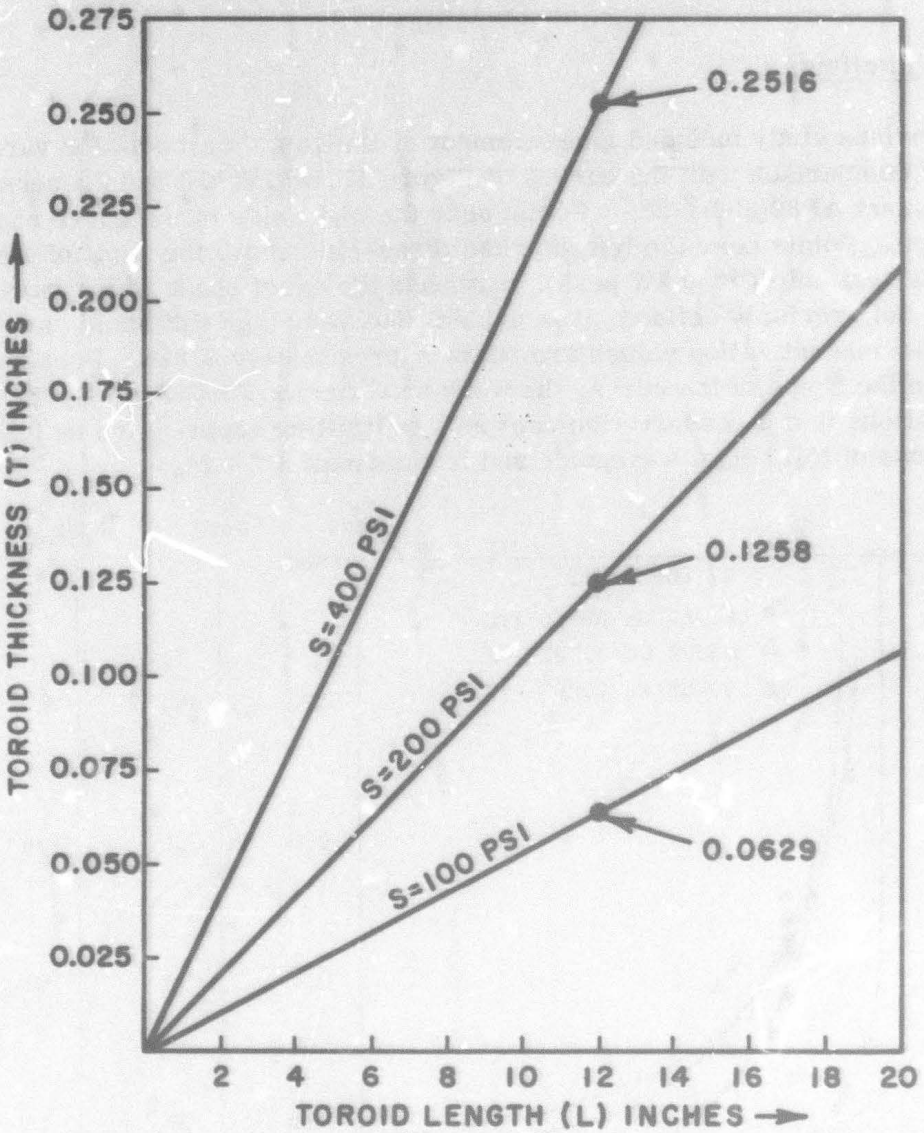

Figure 10. Toroid Dimensional Relationships Vs Thermal Stresses at 500 Watts Dissipated, Assuming Internal and External Cooling

In interpreting the curves, it must be borne in mind that toroid dimensions are critically dependent on phase and loss requirements, and cannot be independently adjusted to achieve optimum thermal properties. Toroid length is limited by maximum loss considerations. Minimum cross section is controlled by phase. Preliminary microwave measurements and calculations indicated that a 24-inch length was the maximum practical value, both from microwave loss and mechanical considerations.

2.5.3 Limiting

The previous study included measurement of limiting thresholds for various materials, for comparison with the curves of Figure 11, which had been generated earlier on Contract AF30(602)4122.[3] Points near the right side of the curve showed good correlation. Points near the left side had thresholds above the limit of the high power facilities available (>230 kW peak). Although the exact shape of the curve near the left side is not precisely defined, it is evident that very high thresholds are attained when normalized magnetization values are below approximately 0.275. Because of uncertainties in the shape of the curve, the work on Contract F30602-67-C0004[1] resulted in recommendations that a conservative approach to limiting suppression be followed, including both use of full height waveguide and low normalized $4\pi M_s$.

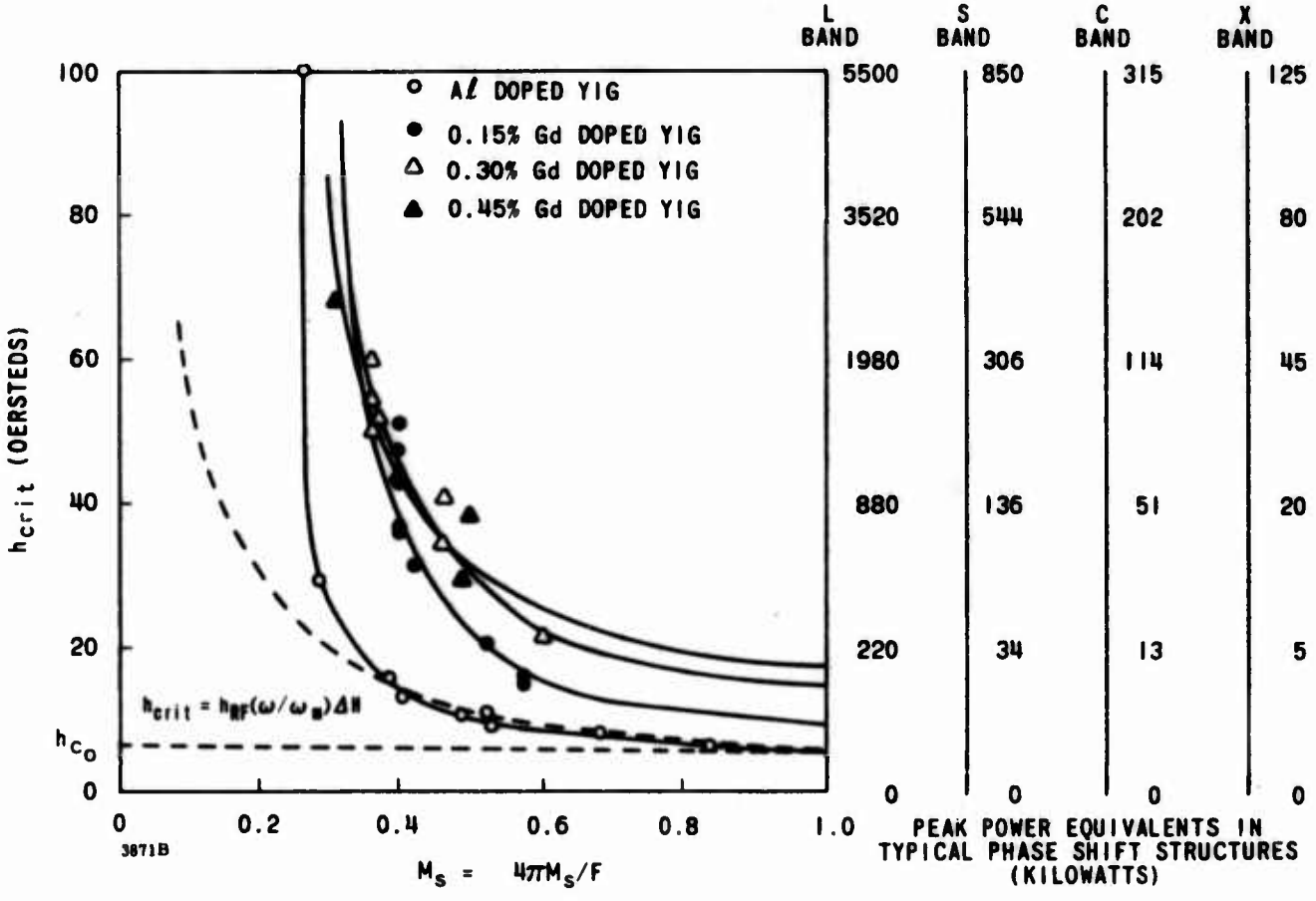

Figure 11. Limiting Thresholds for Various Materials

2.5.4 Breakdown

Contracts F30602-67-C0004[1] and F30602-68-C0006[2] both showed that relatively high breakdown levels could be achieved if air gaps between toroids, cores, and waveguide are either totally eliminated or filled with a high dielectric strength potting material, such as Sylgard 184.

This prior work showed that the breakdown capability of 0.875-inch high waveguide was marginal at 250 kW peak, and for this reason full height (1.340 inches) waveguide was recommended for the present program. Breakdown capability of 1 MW had been attained with this type of construction in a C band phaser at a 2.5-μsec pulse width on Contract F30602-68-C0006.

Scaling from this figure, using the formula:

$$P\ (\text{breakdown}) \propto \left(\frac{\lambda}{\lambda_g}\right)\left(\frac{g}{p}\right)^{1/3}\ \left(\frac{2500}{r}\right)^{1/15}\ \left(\frac{1}{ab}\right)\left(P\right)^2$$

where

$g = \dfrac{2.2 \times 10^4}{f}$

P = relative internal pressure

p = pulse width

r = repetition rate

f = frequency in MHz

λ and λ_g = free space and guide wavelength

a and b = cross-sectional dimensions of guide

and, assuming differences in repetition rate and distance from cutoff are insignificant, indicates that, with one atmosphere overpressure in the S band waveguide:

$$\frac{\text{Breakdown S band}}{\text{Breakdown C band}} = \left(\frac{2.5}{40} \times \frac{5.650}{3.300}\right)^{1/3} \left(\frac{1.0 \times 1.340}{0.650 \times 0.822}\right) \left(2\right)^2 = 4.76$$

$$\text{Breakdown S band} = 4.76 \text{ (C band value)}$$

$$= 4.76 \times 1.050$$

$$= 5 \text{ MW}$$

This figure, though recognized as optimistic, was considered indicative that the tentative cross section selected was adequate.

2.5.5 Higher Order Modes

A full-height phaser configuration was determined to be capable of higher order mode propagation, resulting in insertion loss "spikes" under some circumstances. Computer studies indicated that the more important higher order modes could probably be prevented by proper choice of dielectric constant in the core.

2.5.6 Other Findings

The prior program showed that magnetostrictive effects played a significant role in determining the sensitivity of phase shift to average power. CVB (calcium vanadium bismuth) garnets were shown to be appreciably less sensitive to average power heating because of their lower magnetostrictive constants.

Phase shift per inch was found to be adjustable over a wide range by adjustment of core material and toroid wall thickness. Essentially flat phase versus frequency characteristics are attainable in each case by adjustment of waveguide width. Design curves permitting selection of optimum parameters were generated.

2.6 ELECTRONIC DRIVER

Because of the moderately long switching time (when viewed from typical latching phaser requirements), the driver for the phase shifter was placed at a low priority level. A suitable breadboard driver was constructed to obtain phase measurements.

Because of the large coercive field, H_c, and typically poor B-H loop characteristics of CVB and low $4\pi M_s$ YIG materials, it was determined that the driver needed to deliver very large pulse currents, in the order of 25 to 100 amp.

For laboratory use, three methods of drive can be used:

1. Capacitor discharge . . . For saturation drive only; lab tool only;

2. Transistor pulse circuitry . . . Requires parallel transistors to attain current; typically transistors are slow but will meet specification requirements, and

3. SCR circuitry . . . Similar to capacitor discharge circuitry but could be developed into full driver; employs SCR as trigger for capacitor discharge circuit.

The breadboard driver employed parallel 2N3445 transistors and included an adjustment whereby current could be set to the desired level. This driver had a peak current capability of approximately 60 amp.

SECTION III

ACTIVITY UNDER CURRENT CONTRACT F30602-68-C-0143

3.1 INITIAL DEVELOPMENT STUDIES

Because of the need for internal as well as external cooling to maintain reasonable toroid temperature, the following design criteria were imposed:

1. Reduce toroid wall thickness to a minimum;

2. Core material should be good thermal conductor;

3. Cooling to waveguide side walls was necessary, and

4. Use maximum practical height of waveguide to assure optimum design for limiting arc-over.

Unfortunately, most of the above design requirements oriented to high power operation are in partial opposition to good phase shifter design. Typically:

1. As toroid wall thickness is decreased, phase shift/inch decreases at a rate greater than insertion loss/inch, thus producing higher overall phaser loss.

2. A good thermal conductor material such as boron nitride has a relatively low dielectric constant, resulting in low phase shift/inch when used as a core material within the toroid.

3. Cooling structure from toroid to side wall also possesses some dielectric constant ($\epsilon \approx 4.5$). For this application, low dielectric constants ($\epsilon \approx 1$) are desired; the higher value of $\epsilon = 4.5$ results in approximately 10 percent loss in phase/inch.

4. The width of the core must be maintained at a value compatible with internal cooling.

5. Increase in height beyond $0.3\ \lambda_g$ leads to the possibility of moding in the loaded structure.

6. Because of the rigidity of the internal cooling structure (which also becomes the charging wire), construction takes the form of a split core and split toroid.

Within the limits of the above constraints, an additional series of computer runs was made to determine configuration for zero phase slope, etc. These runs were also oriented towards the optimization of the unit within the limits imposed, especially in the areas of phase shift per inch and insertion loss.

3.2 HARDWARE DESIGN

The cross section chosen from the computer data of paragraph 2.5.4 is shown in Figure 12.

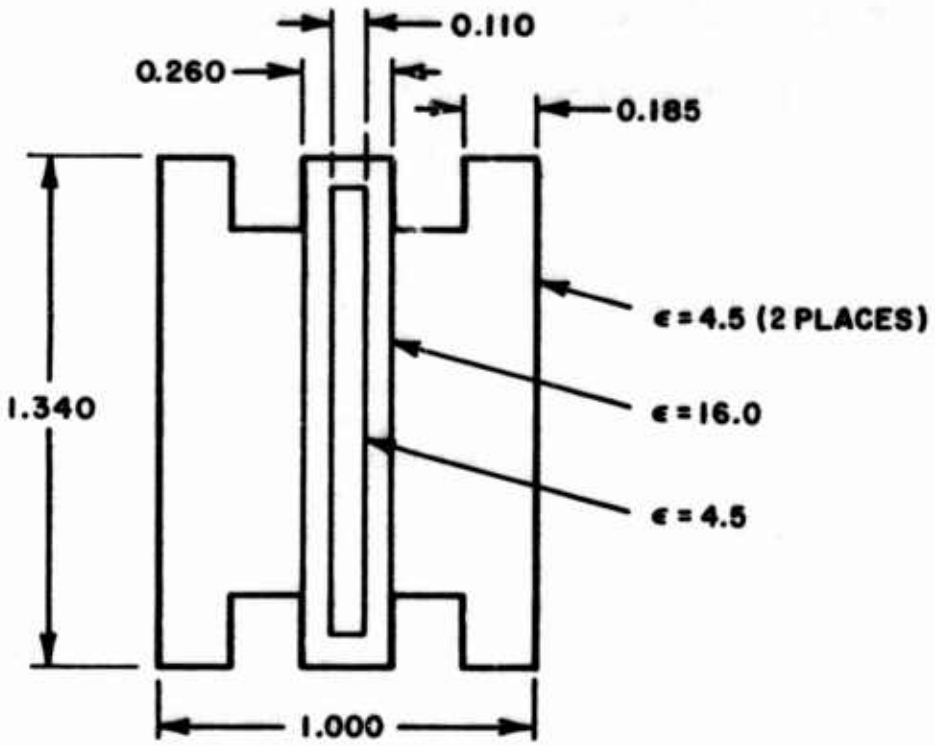

Figure 12. Chosen Computer Cross Section

When transformed into a suitable piece of hardware, the cross section becomes that of Figure 13.

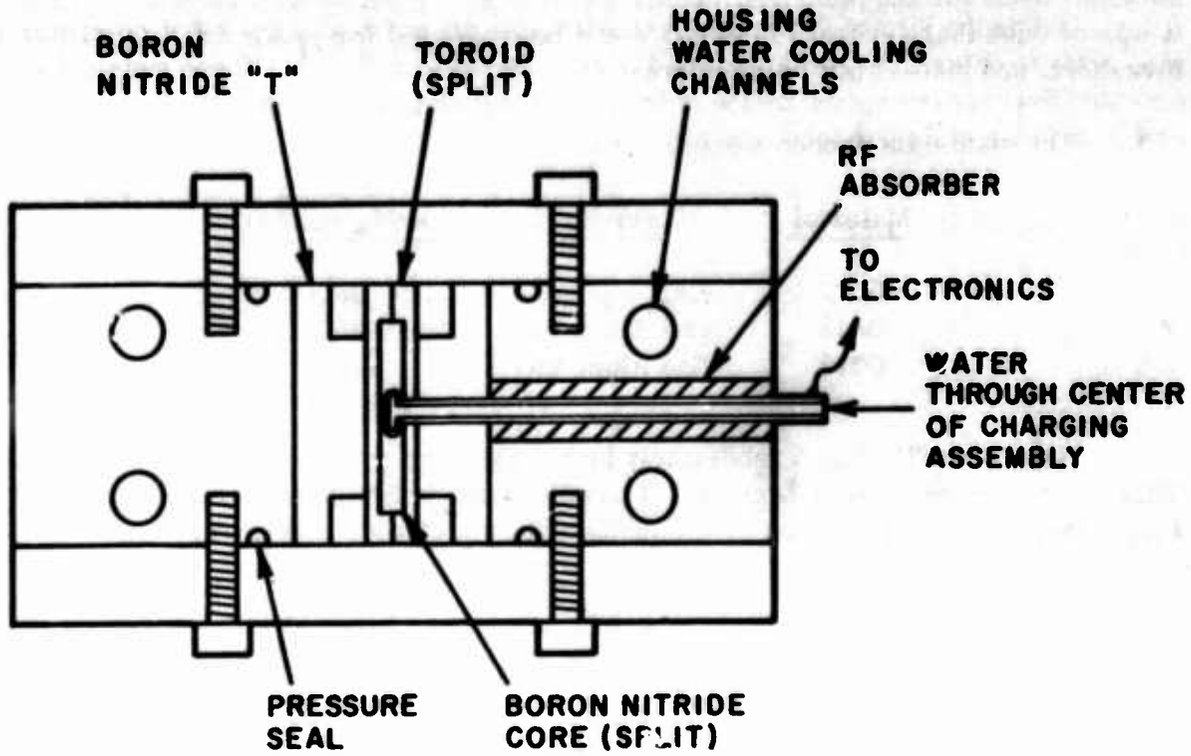

Figure 13. Computer Cross Section Transformed into Practical Hardware Cross Section

Note that to reduce continuity of gaps in toroid/core surfaces to a minimum consistent with good arc-over practice, the core is split parallel to the broad wall whereas the toroid is split parallel to the narrow wall. Not only can assembly be thus attained but such toroid splitting permits the internal grinding of the toroid required for excellent toroid-core fit. Use of boron nitride as the core material offers the advantage that hand-fitting to essentially zero tolerance can be attained as boron nitride is a soft, easily shaped material.

3.2.1 Material Choice

As discussed in Section 2, two possible material choices were available; that is, aluminum-gadolinium doped YIG and calcium vanadium bismuth material (CVB).

In addition, the curve of Figure 11 shows a relationship between peak power and h_{crit} which is only true for the cross section chosen for experimental study; that is, the cross section of Figure 14. Although approximate correlation of limiting for the cross

section chosen for the polarizer phaser element was possible on a mathematical basis, it was decided that several materials would be evaluated for power handling, limiting threshold, and phase shift parameters.

The materials chosen were:

Material	Family	$4\pi M_s$ (gauss)
G437	CVB	280
G518	Gad Alum YIG	250
G312	Gad Alum YIG	410

Note that G312 has a moderately high $4\pi M_s$ ($m_s \approx 0.383$) for this application. This choice was made to determine, if possible, the relationship between h_{crit} and P_{peak} that would probably not be attainable with the other material choices.

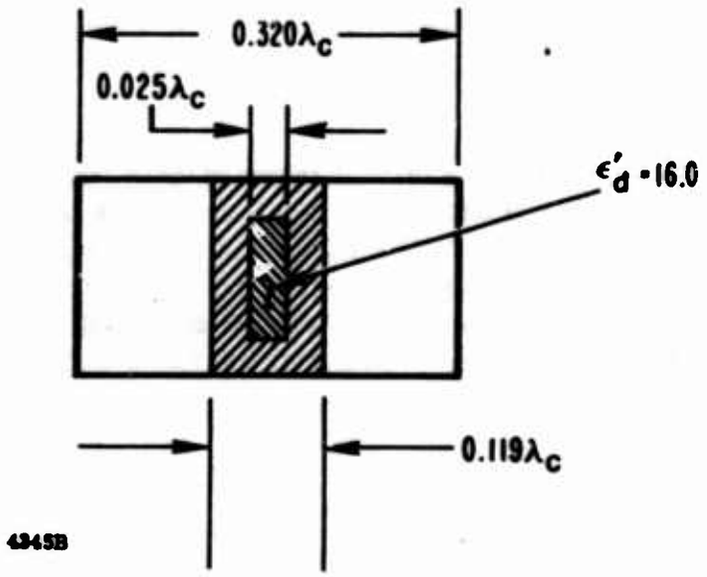

Figure 14. Typical Phase Shifter Cross Section

3.2.2. Hardware Fabrication

Four test structures were fabricated, two with charging wire-cooling structures and two without. The units without charging wire-cooling structures were to be used as a control for studying the arc-over effects of this metallic part within the waveguide.

The units were designed with waveguide cooling separated from charging structure cooling, again for studying the effectiveness of this structure in removing internal heat.

All units were designed for pressurization. A special absorber design was used where the charging wires penetrated the waveguide wall which would not only isolate the wire electrically from the waveguide, but would also act as an rf absorber while assuring proper sealing for pressurization.

3.3 TESTING

The structures were evaluated in four basic stages:

1. Mechanical: check for pressurization, water leaks, etc.;
2. Low level evaluation: insertion loss, VSWR, differential phase, etc.;
3. Medium power evaluation: to 200 kW peak and 900 watts average, with various coolant configurations, and
4. High power: various power levels, peak and average, various pulse lengths.

3.3.1 Mechanical Evaluation

Pressurization techniques proved adequate. It was found that although the pressure to obtain adequate waterflow through the charging wire-cooling structure was reasonable, due to the necessary increase in length of final unit, the pressure necessary was quite high. This could be remedied in the final design by using a plated, stainless steel, thin wall structure, thereby increasing internal waterflow cross section with no further compromise of rf properties.

RF suppressor design was adequate.

3.3.2 Low Power Evaluation

Low power evaluation of the four test units included the following:

1. VSWR vs frequency;

2. Loss vs frequency, and

3. $\Delta\phi$ (saturation drive).

Each of the four units was evaluated for insertion loss and VSWR over the frequency band 3.1 to 3.6 GHz. Plots of these data are given in Figures 15 and 16. It is interesting to note that of the two toroid lengths evaluated, no appreciable increase in loss is associated with the longer of the units. It can thus be assumed that only a small portion of the loss is associated with the dielectric and magnetic losses of the toroid itself. It could also be assumed that increasing unit length to that necessary for 90-degree final hardware would also only slightly increase the loss over the values recorded.

It is also noted that those units with internal charging/cooling structure (units with 12-inch material length) show the effects of this structure in their loss and VSWR plots. The combined causes of full height waveguide and large charging structure result in a high probability of moding.

The phase shift of the units with charging structures is as follows:

$$G437 \approx 37^{\circ}/12 \text{ in.} \approx 3.1^{\circ}/\text{in.}$$
$$G518 \approx 48^{\circ}/12 \text{ in.} \approx 4.0^{\circ}/\text{in.}$$

The above values were measured using a capacitor discharge driver which yields high currents and essentially saturated drive.

Note that although the $4\pi M_s$ of G437 (280 gauss) is higher than that of G518 (250 gauss), the phase shift was appreciably lower. This is the typical result of low remanence ratio B_R found for the CVB family of materials. This material was chosen not for its remanent properties, but because of its essentially zero magnetostrictive properties and as such could yield acceptable phase shifts under such an environment as encountered in the polarizer.

G312 (410 gauss $4\pi M_s$) was not checked for phase shift since it was used only in a housing without charging wire. This material was chosen only for limiting study which will be discussed in later sections. It would be reasonable to assume, however, that phase shift for this material would approach 6.6°/in. because of its higher remanent magnetization.

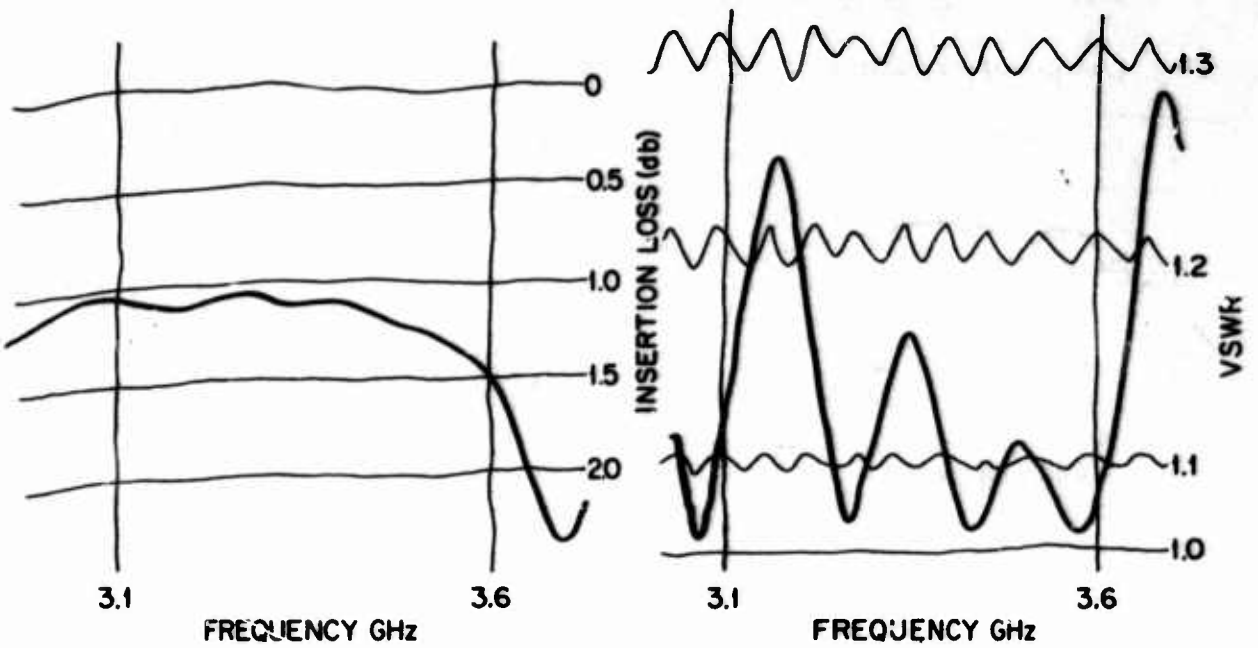

Material G518 Material G518

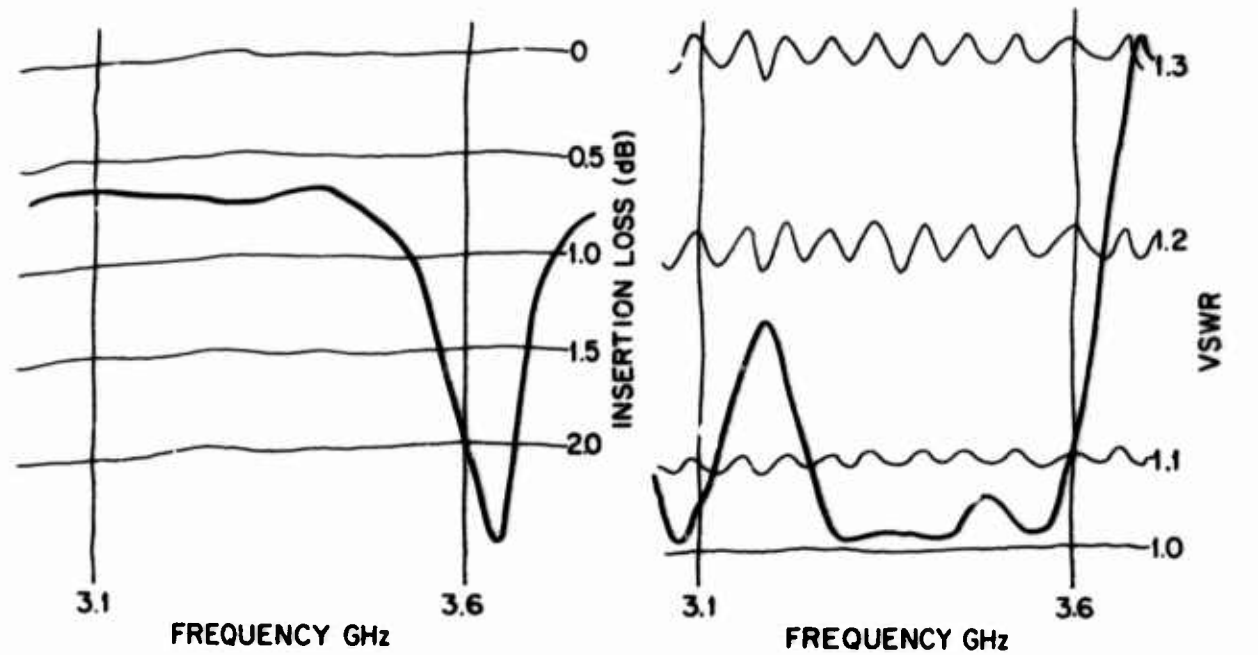

Material G312 Material G312

Figure 15. Plots of Insertion Loss and VSWR Vs Frequency. 6-Inch Toroid Lengths. No Charging/Cooling Structure.

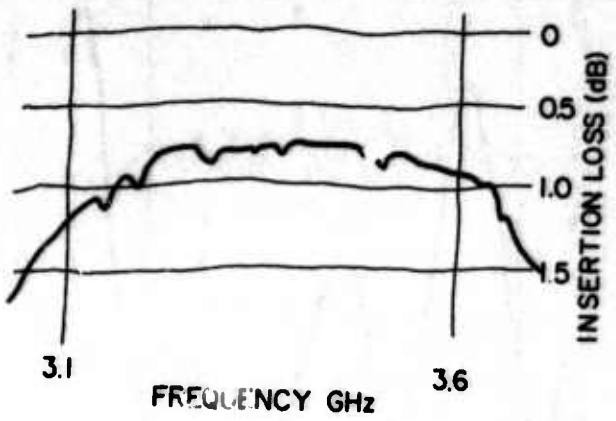

Material G437

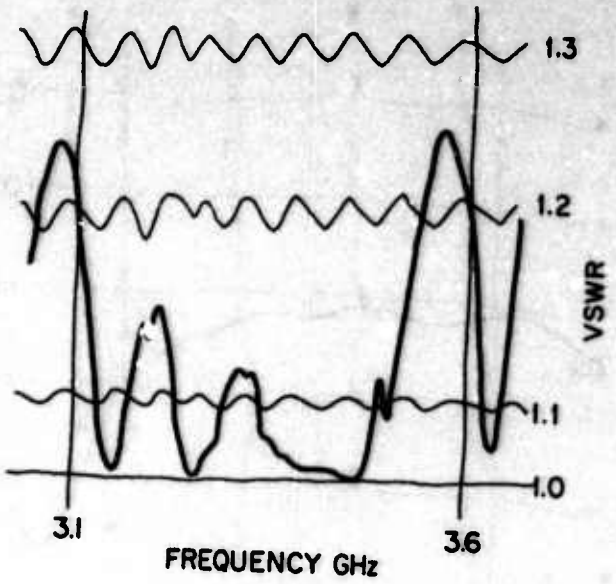

Material G437

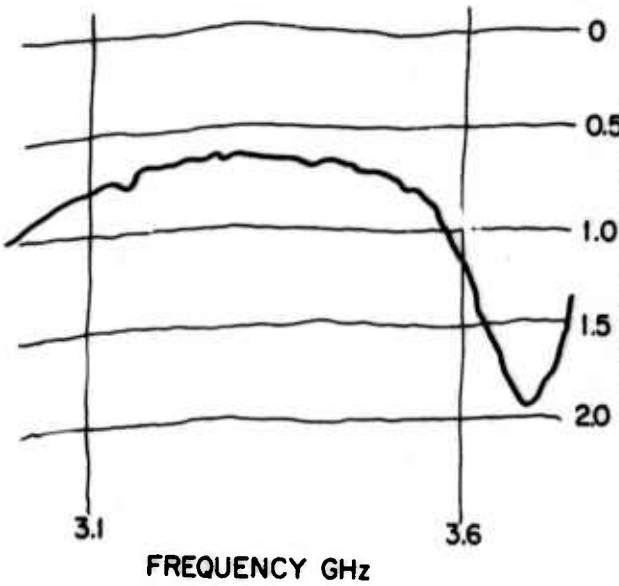

Material G518

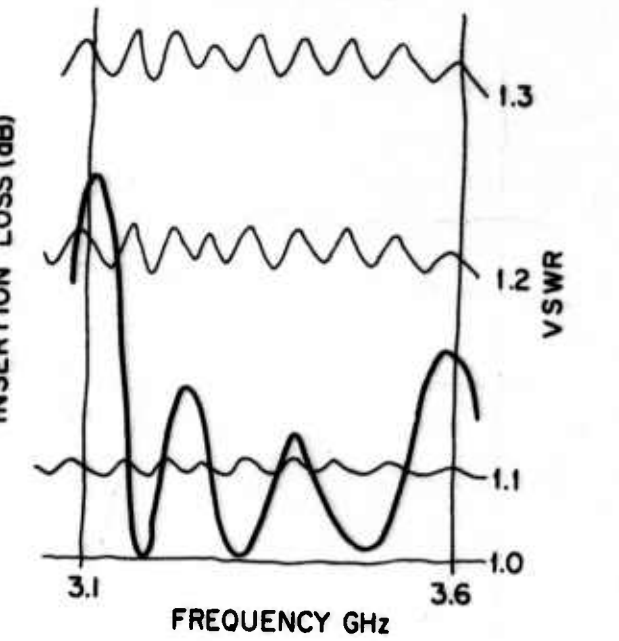

Material G518

Figure 16. Plots of Insertion Loss and VSWR Vs Frequency. 12-Inch Toroid Lengths. With Charging/Cooling Structure.

3.3.3 Medium Power Evaluation

The four test units were checked under one or more of the following conditions:

1. Average power to 900 watts (cw);

2. Short pulse peak power (250 kW peak, 1 μsec), and

3. With and without water cooling through the charging structure.

The units were checked for phase degradation with power and limiting.

Under these test conditions, all units survived the testing with no physical or electrical damage. In addition, all units (including that with G312 material) showed no signs of limiting at peak powers to 250 kW.

Phase shift as a function of average power and phase shift at 900 watts average as a function coolant flow through the charging structure were measured for the units containing G437 and G518 materials. These data are given in Figure 17. From these data, it is clearly seen that for average powers in excess of 1000 watts, core cooling is not only advisable but necessary, and that the chosen design is effective in reducing temperatures within the structure.

3.3.4 High Power Testing

The four test units were high-power evaluated at Microwave Associates, Tube Division, Burlington, Massachusetts on April 28 to 30, 1969.

The units were rematched to produce adequate VSWR responses in the available high power frequency range of 2.8 to 3.1 GHz.

For convenience, each unit has been designated by a serial letter as tabulated below. Also given are material parameters of each material for easy cross reference.

Unit	Toroid Length	SMED Matl. No.	$4\pi M_s$	ΔH	Tan δ	ϵ	Composition
A	12 in.	G437	280	210	0.0007	17.1	CVB
B	12 in.	G518	250	130	0.0006	14.9	Gd Al YIG
C	6 in.	G518	250	130	0.001	14.9	Gd Al YIG
D	6 in.	G312	410	105	0.0008	14.9	Gd Al YIG

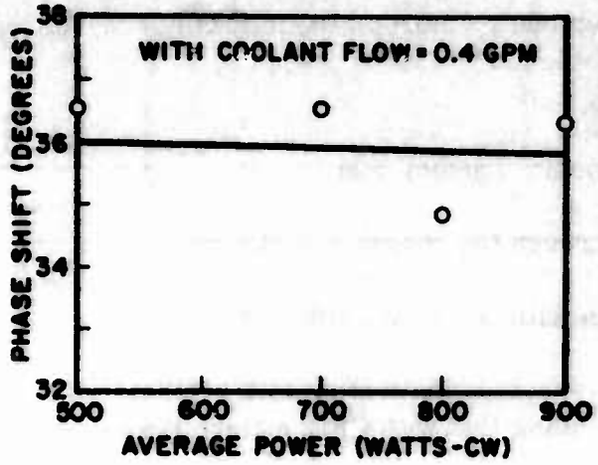

MATERIAL G437 (CVB)

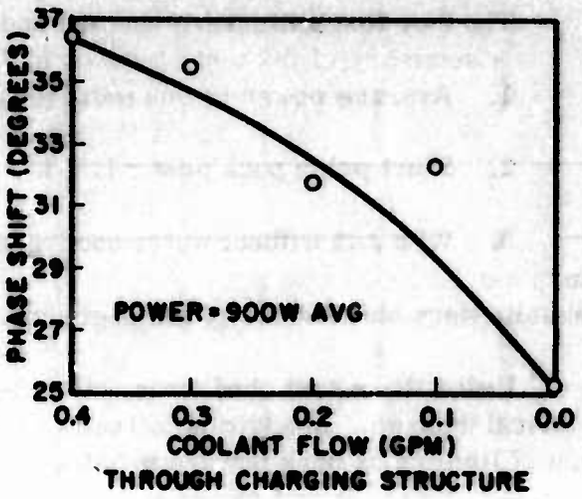

MATERIAL G437 (CVB)

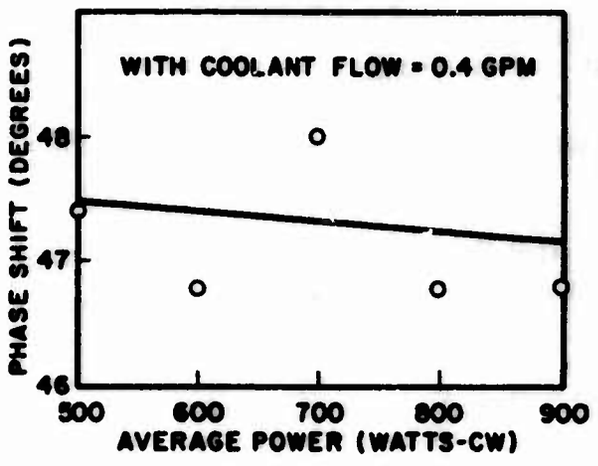

MATERIAL G518 (Gd Al YIG)

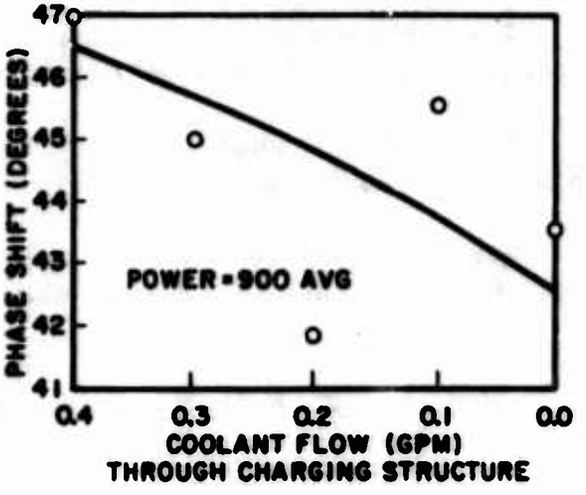

MATERIAL G518 (Gd Al YIG)

Figure 17. Phase Shift Vs Average Power and Coolant Flow. 12-Inch Toroid Lengths.

All units arced during the test. The units without charging structures withstood power levels higher than those with charging structures.

A summary of the tests is given in Table III.

Table III. High Power Test Results

Unit	A	B	C	D
Max power at 2-μsec pulse, 25 psi air in guide	1.0 MW	0.5 MW	3.0 MW	3.0 MW
Max power at 30-μsec pulse, 25 psi nitrogen	---	---	0.86 MW	---
Arc level (MW)	1.0	0.5	0.77	3.0
Pulse width when arced (μsec)	2.0	2.0	30.0	2.0
Pressure when arced (psig)	25	25	25	15
Limiting observed	No	No	No	No
Typical loss, dB	1.0	1.0	1.0	1.0
Phase shift at 0.25 MW	---	39.4^{o}	---	---
Phase shift at 0.5 MW	41.1	---	---	---

The 2-μsec pulse width tests were conducted at 2.8 GHz, and were performed to examine limiting and breakdown characteristics. No limiting occurred, even in the unit with G312 which has a relatively high $4\pi M_s$. This result would indicate that because of the full height and reduced loading factors that the relationship between h_{crit} and peak power originally used was conservative and that the higher $4\pi M_s$ material with greater phase activity would be acceptable.

Unit D was "deliberately" arced in the 2-μsec pulse set up by reducing pressure in successive 5-psig steps to permit extrapolation to a safe pressure-power combination to use in later 30-μsec pulse tests. Units A and B (those units with charging structures) broke down at unexpectedly low power levels and only one phase data point could be taken on each.

The wide pulse tests were conducted at 2.91 GHz. Unit C, the only surviving unit after 2-μsec testing, was evaluated. It withstood 0.86 MW peak, 5.15 kW average without arcing when pressurized with 25-psig nitrogen. With 25-psig air, however, it broke down at 0.77 MW peak, 4600 watts average.

When disassembled, all units showed the same type of damage. Arc tracks were confined to the toroid-matching transformer interface (across the end of the toroid) except in Unit C which arced at 30-μsec pulse. In Unit C, the Rexolite matching transformer at the input end was also badly burned and caused a large amount of soot to be deposited over the waveguide interior. This burning of the Rexolite would indicate the need for all ceramic transformers at high power levels. The burn indicated not only arcing damage due to high peak powers, but also disintegration due to high temperatures generated by losses within the structure. (Note: the transformers are not cooled.)

Figures 18 through 24 show the interior appearance of the units after disassembly and include closeups of typical arc damage.

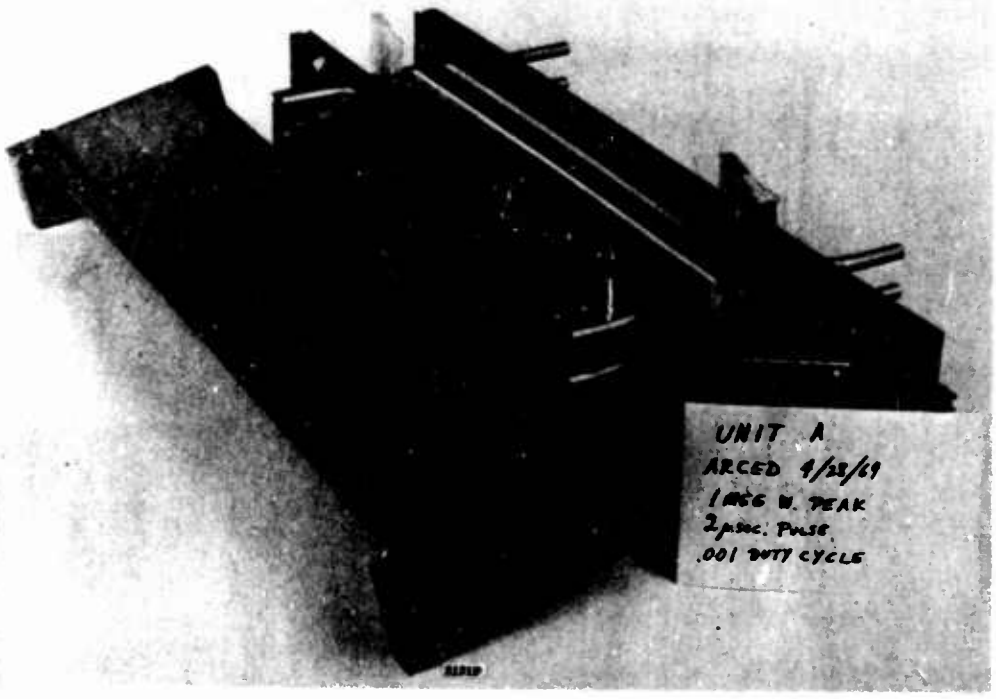

Figure 18. Unit A after Disassembly

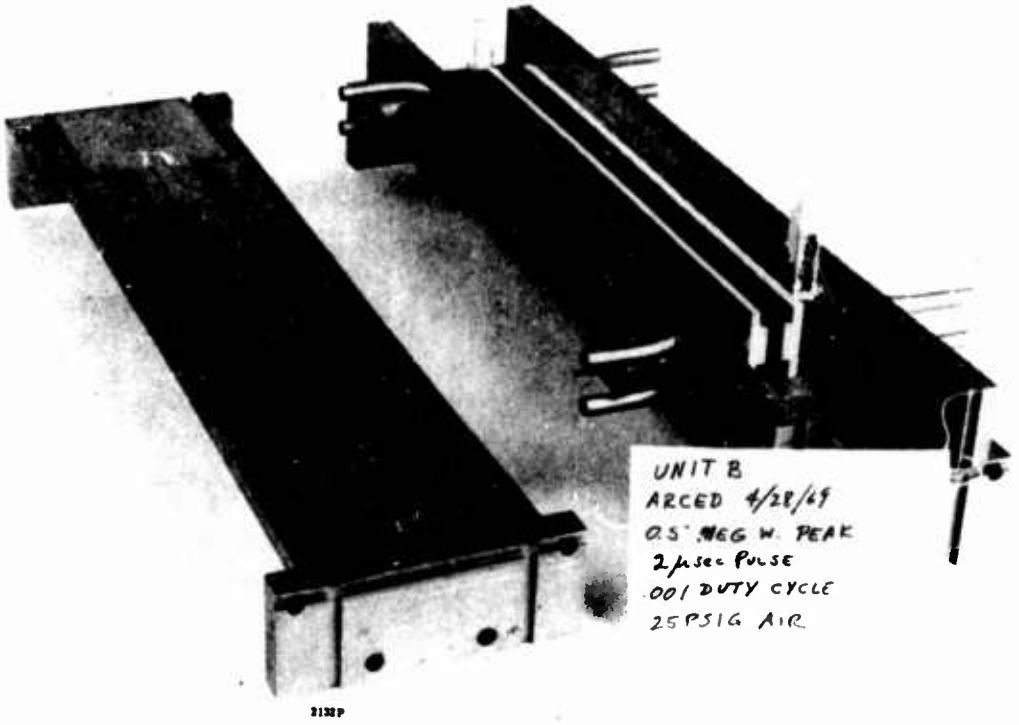

Figure 19. Unit B after Disassembly

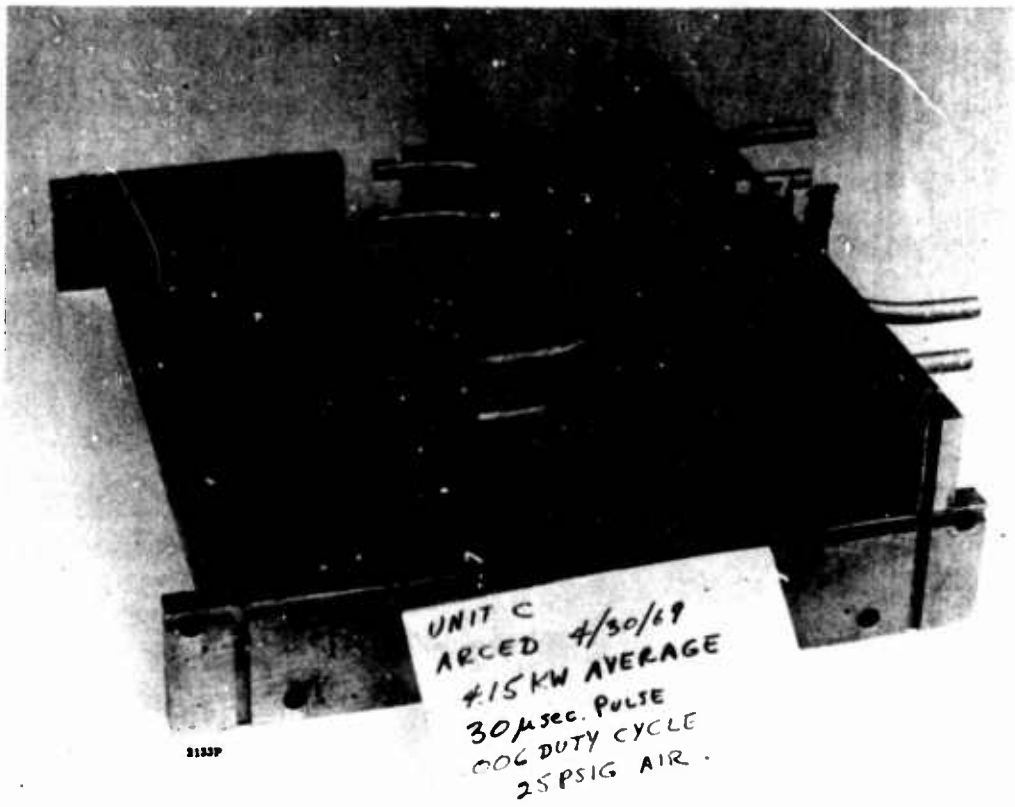

Figure 20. Unit C after Disassembly

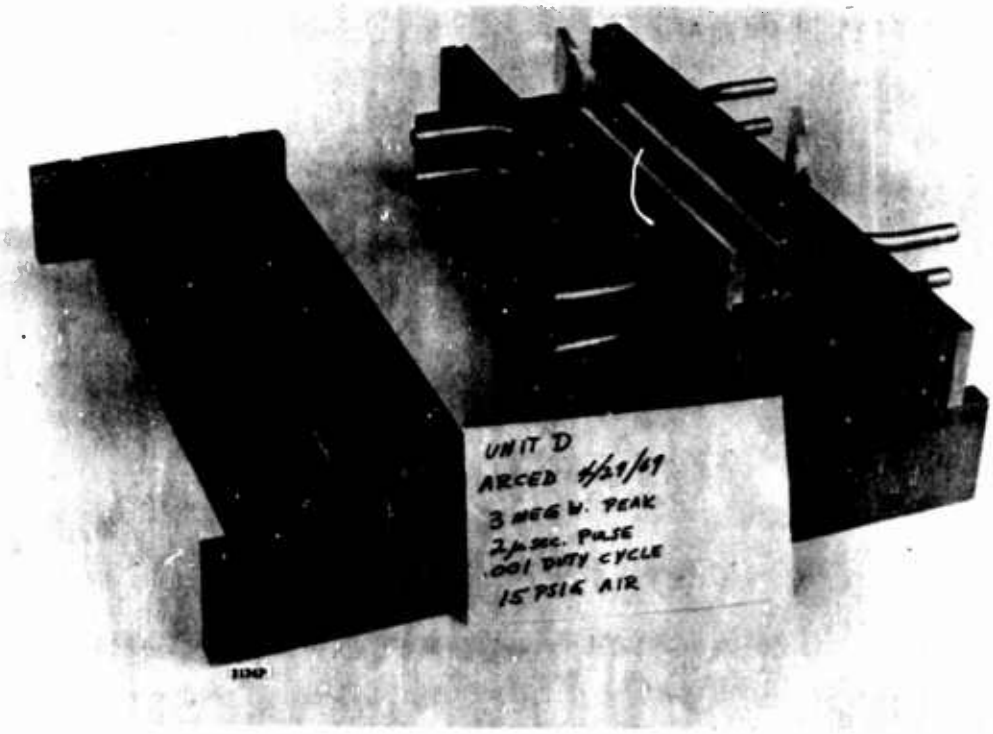

Figure 21. Unit D after Disassembly

Figure 22. Input Transformer of Unit C

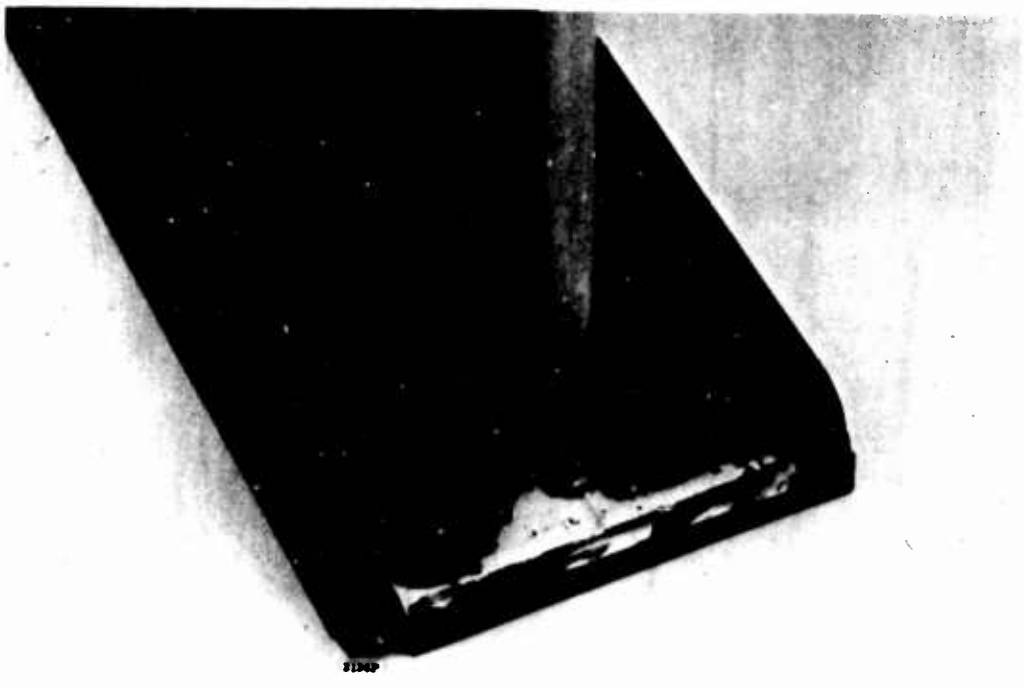

Figure 23. Closeup of Arcing and Toroid Breakage at Toroid-transformer Interface

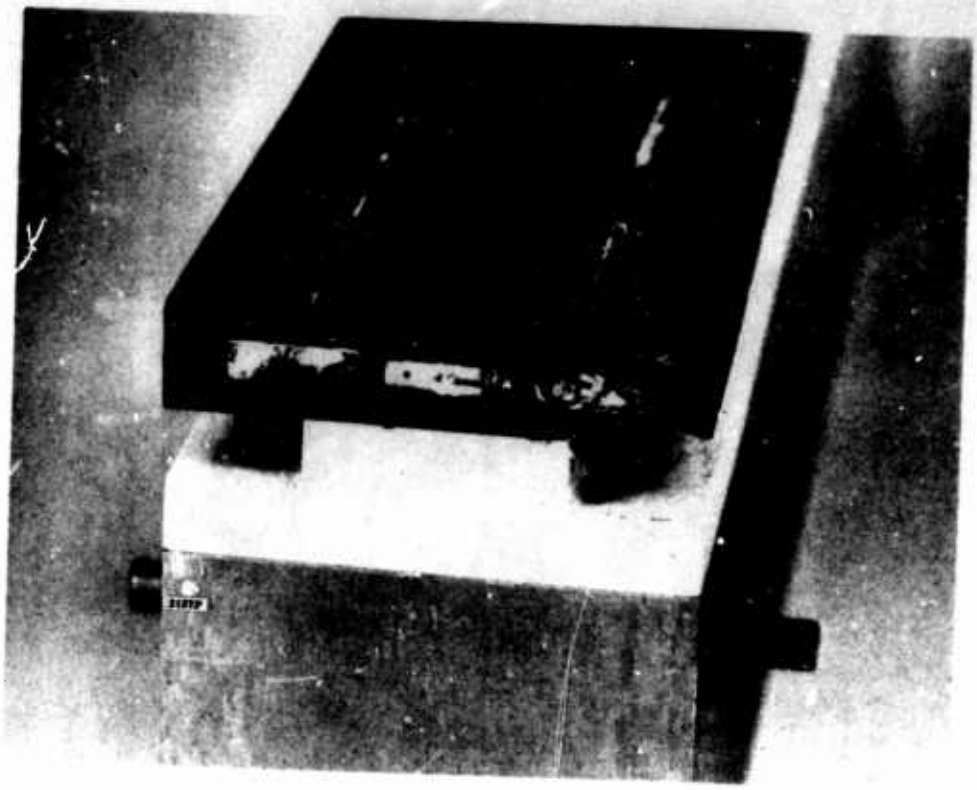

Figure 24. Closeup of Arcing at Toroid-transformer Interface

SECTION IV

CONCLUSIONS AND RECOMMENDATIONS

4.1 GENERAL

As a result of the high power testing, the program was re-evaluated as to the probability of success with redesign within the present time/dollar scope of the contract. The probability of attaining the design goals of the program was considered of sufficiently low level that the recommendation was made to terminate the contract with completion of this final report summing results to date.

4.2 FINDINGS AND CONCLUSIONS

1. The ferrites selected do not limit, up to 3-megawatts peak.

2. Insertion loss tends to decline slightly with increasing power. This is believed to be a temperature effect.

3. The insertion loss of a typical 90-degree phase element even for redesigned units would be approximately 1.0 dB.

4. Presence of the charging-cooling structure aided phase performance but has a noticable adverse effect on breakdown. It is believed that this is a result of excitation of "hybrid," or cross-polarized modes by a combination of the presence of charging wire within the structure and use of full height waveguide.

5. Arc damage is confined almost exclusively to the toroid-matching transformer interfaces, whether there is a charging wire or not. This same effect was noted at C band under Contract F30602-68-C-0006,[2] RADC-TR-68-557, and as noted, does not appear to be related to the abrupt waveguide width discontinuity.

6. Substitution of air for nitrogen or reducing air pressure both result in reduced breakdown levels.

7. No significant workmanship defects were found when the units were disassembled and inspected. Small adhesive voids about 0.015 dia were found in corners. However, the relation between these and arcing, if any, was totally destroyed along arc paths.

8. Some ferrite breakage was evident at the end of the toroids where arcs occurred. Additional breaks occurred during disassembly for inspection, probably because considerable force was necessary to overcome adhesive bonds.

9. Redesign of the unit would most likely be oriented to the use of the higher $4\pi M_s$ garnet material possibly in a reduced height structure to suppress "hybrid" moding. It is questionable, however, if this redesign would be capable of approaching the design goals of this program.

4.3 RECOMMENDATIONS

The concepts of the polarizer design using latching phase shift elements to attain high speed polarization switching are sound. The use of power splitting with known recombinations for all polarizations is especially advantageous in that each element of the system is subjected to equal powers at all times, thus assuring stability.

Because of the phase element nonreciprocity, duplexing is inherent in the structure.

The results of this investigation also indicate that phase shifters capable of handling very large peak and average powers may be designed at some future time. However, the present state of the art, both in ferrite materials and unit construction, is not far enough advanced to achieve these goals.

As a result, it has been recommended and accepted that this contract be terminated until such time as the probability of success is increased by further developments in phaser and material technology.

REFERENCES

1. Sperry Microwave Electronics Company: "Variable Polarizer," Final Report on Contract F30602-67-C0004. RADC-TR-67-601, December 1967.

2. Sperry Microwave Electronics Division: "High Power C-Band Phase Shifters," Final Report, Contract F30602-68-C-0006. RADC-TR-68-557, October 1968.

3. Sperry Microwave Electronics Division: "Continued Studies on Advanced Ferrimagnetic Materials Applied to Digital Phase Shifters," Final Report on Contract AF30(602)4122, May 1967. Sperry Report No. SJ-220-4002-6.

APPENDIX I

A SUMMARY OF THE GEOMETRICAL PROPERTIES OF THE POLARIZATION ELLIPSE

ELLIPTICAL POLARIZATION

A SUMMARY OF THE GEOMETRICAL PROPERTIES OF THE POLARIZATION ELLIPSE

1. INTRODUCTION

1a. Definition of Elliptical Polarization

The description of an elliptically polarized wave is usually simplified by breaking the wave down into two separate components and treating them separately. These two components generally take one of two forms:

(1) Two linear waves whose polarization planes are in space quadrature and which exhibit an arbitrary amplitude and phase difference.

(2) Two circularly polarized waves of arbitrary amplitude and phase rotating in opposite directions.

Throughout this discussion we shall consider only the linear components of case (1), propagating along the positive z-axis, and at the same frequency.

The resultant of the E vectors of the two component waves will in general spiral about the axis of propagation at the component wave frequency, varying in amplitude at twice the component wave frequency.

If we allow the resultant wave to pass through a plane perpendicular to the direction of propagation, the tip of the E vector will, in general, trace out the figure of an ellipse. It is this characteristic which in fact gives rise to the terminology. The sense of rotation of the E vector in the plane of projection determines whether the wave is "clockwise" or "counterclockwise." Stated more exactly: A wave is elliptically polarized in the clockwise sense if the projection of the E vector of a wave progressing toward the observer rotates in the clockwise direction.

Confusion often arises at this point due to the fact that various writers assume different points of observation when describing rotation. In many discussions of polarization it is not clear whether one is speaking of rotation in the projection plane or in space or for that matter which side of the projection plane is being observed.

We shall always consider propagation toward the observer, along the positive z axis and in a standard right-hand coordinate system. Our plane of projection may then be chosen as the X Y-plane in its standard orientation.

1b. Basic Geometric Definitions

It will be the purpose of this memorandum to describe in detail the properties of the polarization ellipse. To avoid any later problems in notation we shall here define our system as completely as possible.

Figures 1a and 1b indicate our basic coordinate system, the z axis is out of the drawing plane. Figure 1b also indicates a rotated coordinate system (X_R Y_R) and the angle β by which we shall measure the degree of rotation. The conventional quadrant notation is also shown.

Figure 2 shows a polarization ellipse of some general size and orientation as it might appear on the XY-plane. The purpose of the system X_R Y_R is now clear, the angle β is always chosen to align the rotated system with the axes of the ellipse.

From Figure 2 and the previous paragraph we may specify the important quantities to be used in describing the ellipse, they are:

(1) E_x, E_y - the amplitude constants of the two orthogonal waves.

(2) β - the angle which the major axis forms with the X axis.

(3) 2a, 2b - the major and minor axes of the ellipse.

(4) δ - the phase angle between the two component waves.

(5) $\tan \alpha = \frac{E_y}{E_x}$ = the amplitude ratio

(6) $\tan \chi = \frac{b}{a}$ = the axial ratio of the ellipse.

(7) The direction of rotation around the ellipse.

1c. Selection of Approach

For the purpose of this discussion we shall assume that an elliptically polarized wave is composed of two orthogonal linear waves of arbitrary amplitude and

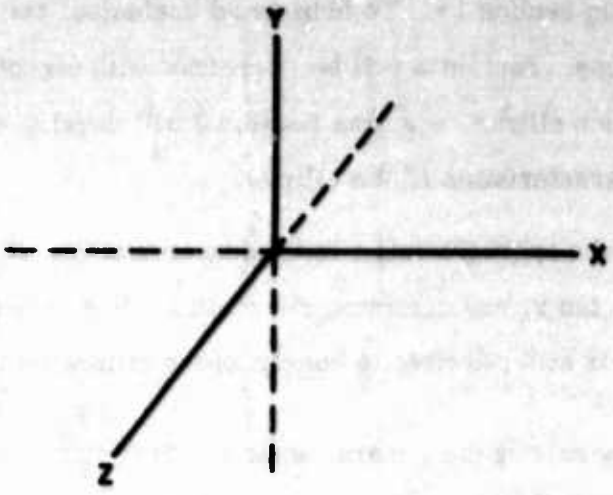

(a) The Coordinate System Used in This Analysis

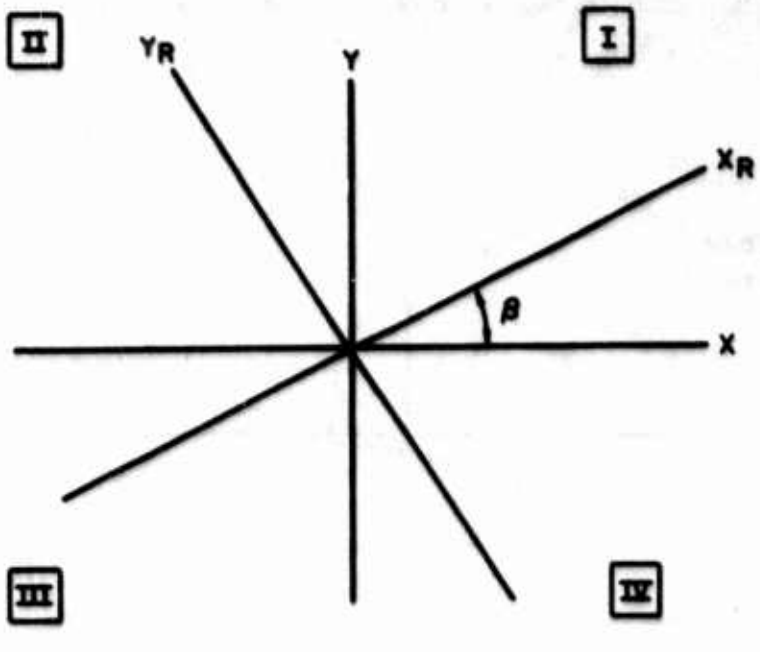

3418B

(b) β, The Angle of Axis Rotation

Figure 1. Definition of Coordinate Systems

phase as described in Sectica 1a. To help avoid confusion, the analysis is divided into two main sections. Section 2 will be concerned with directly deriving the equation of the polarization ellipse, whereas Section 3 will develop expressions for each of the important characteristics of the ellipse.

In general the approach taken is to assume that E_x, E_y and δ are known and then to solve for β, $\tan\chi$, and direction of rotation. If δ is not known and only β and $\tan\chi$ are known, it is still possible to construct the ellipse so that its relative dimensions are correct by solving the general equation (5) for $\frac{E_y}{E_x}$. For this purpose E_x and E_y may be expressed as a "normalized ratio" $\frac{E_y}{E_x}$, where $E_x = 1$ without changing the following analysis.

The relationships between the several variables and a discussion of three examples appears in Section 4.

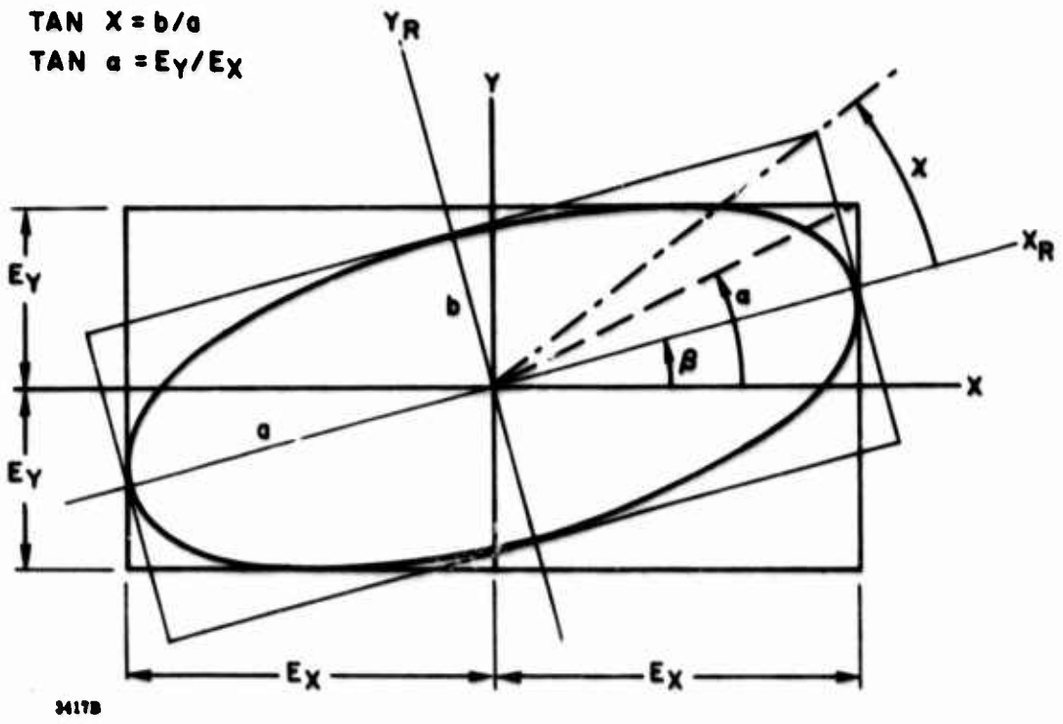

Figure 2. Definition of the Various Terms Used in This Analysis

2. DERIVATION OF THE POLARIZATION ELLIPSE

2a. The General Equation

Consider the two orthogonal waves:

$$X = E_x \cos\left[\omega\left(t - \frac{z}{v}\right) + \delta_1\right]$$
$$Y = E_y \cos\left[\omega\left(t - \frac{z}{v}\right) + \delta_2\right] \quad (1)$$

Where E_x, E_y are horizontal and vertical amplitude constants, δ_1, δ_2 are phase angles and $\omega\left(t - \frac{z}{v}\right)$ is in radians expressed as having an arbitrary time origin. X and Y are, therefore, the components of E, the resultant electric vector at any time t. The equations (1) represent a curve traced out by the E vector in the X Y -plane and are termed parametric equations.

Letting $\omega t' = \omega\left(t - \frac{z}{v}\right) + \delta_1$ and $\delta = \delta_2 - \delta_1$, we redefine the time orgin and simplify the equations. We now have:

$$X = E_x \cos \omega t'$$
$$Y = E_y \cos (\omega t' + \delta) \quad (2)$$

Expanding Y we obtain:

$$Y = E_y \cos (\omega t') \cos \delta - \sin (\omega t') \sin \delta . \quad (3)$$

Eliminating $(\omega t')$ from (2) and (3) gives

$$\left(\frac{Y}{E_y} - \frac{X}{E_x} \cos \delta\right)^2 = \left[1 - \left(\frac{X}{E_x}\right)^2\right] \sin^2 \delta$$

which may be reduced to

$$\frac{X^2}{E_x^2} + \frac{Y^2}{E_y^2} - \frac{2 X Y \cos \delta}{E_x E_y} = \sin^2 \delta . \quad (4)$$

By multiplying (4) by $E_x^2 E_y^2$ we may reduce it to a completely general form,

$$E_y^2 X^2 + E_x^2 Y^2 - 2 E_x E_y X Y \cos \delta - E_x^2 E_y^2 \sin^2 \delta = 0. \tag{5}$$

This compares directly to

$$AX^2 + BXY + CY^2 + DX + EY + F = 0 \tag{6}$$

which is the general second degree equation in X and Y.

In our case D = E = 0, and the term in (XY) indicates a rotation in the XY-plane. The determinant of (4) or (5) may be evaluated[2] and predicts the locus of points to be an ellipse. As an aid to plotting the figure we may solve (5) for its (X, Y) intercepts and points of tangency to the lines $X = \pm E_x$ and $Y = \pm E_y$. These points are, respectively, $X = \pm E_x \sin \delta$, $Y = \pm E_y \sin \delta$ and $\pm(E_x, E_y \cos \delta)$, $\pm(E_x \cos \delta, E_y)$. In general these eight points will allow a fairly accurate sketch of the ellipse to be made.

2b. Rotation of the Axes

Referring back to Figure 2 we may draw upon analytic geometry to write a set of transformation equations to go from the X Y-plane to the X_R Y_R- plane or vice-versa, they are,

$$\begin{aligned} X &= X_R \cos \beta - Y_R \sin \beta \\ Y &= X_R \sin \beta + Y_R \cos \beta \end{aligned} \tag{7}$$

$$\begin{aligned} X_R &= X \cos \beta + Y \sin \beta \\ Y_R &= -X \sin \beta + Y \cos \beta. \end{aligned} \tag{8}$$

Applying (7) and (8) to (5) we could obtain a new equation in X_R and Y_R which would not have a rotation term.[4] The equation obtained is rather complicated in appearance and adds little insight into the problem at hand. This method is used, however, to obtain the expression for β given in Section 3a.

3. PROPERTIES OF THE POLARIZATION ELLIPSE

3a. The Inclination of the Ellipse

The evaluation of β may be taken directly from analytic geometry by applying equations (7) and (8) to the general second degree equation (6) and setting the coefficients of the (X Y) terms equal to zero. This approach yields

$$\tan 2\beta = \frac{B}{A - C}, \quad A - C \neq 0. \tag{9}$$

If $A = C$, $\beta = \pi/4$. Applying this to (5) results in the useful expression

$$\tan 2\beta = \frac{2 E_x E_y \cos \delta}{E_x^2 - E_y^2} \tag{10}$$

or

$$\beta = \frac{1}{2} \text{Arctan} \left[\frac{2 E_y E_x \cos \delta}{E_x^2 - E_y^2} \right] \tag{11}$$

If $\tan 2\beta$ is negative, we take 2β in quadrant II, if positive in quadrant I; therefore, we always have $0 \leq \beta \leq \pi/2$. At this point β is the <u>smallest</u>, positive angle of rotation which will align the X_R axis with <u>either</u> axis of the ellipse; this will be clarified further in Section 4.

Equation (10) may be written in a different form by referring again to Figure 2 and defining a new angle α by

$$\tan \alpha = \frac{E_y}{E_x} . \tag{12}$$

From trigonometry $\tan (2\alpha) = \dfrac{2 E_y E_x}{E_x^2 - E_y^2}$, and from (10)

$$\tan 2\beta = \tan (2\alpha) \cos \delta , \tag{13}$$

which will be useful in the next section.

3b. The Axial Ratio of the Ellipse

In this section we shall take a slightly different approach to the solution of the problem by assuming the form of the parametric equations and setting up certain relations which will allow us to express the axial ratio in terms of δ, E_x, and E_y.

Consider the ellipse of Figure 2 as it is situated in the rotated $(X_R\ Y_R)$ system. We may write its equation immediately by inspection; it is

$$\frac{X_R^2}{a^2} + \frac{Y_R^2}{b^2} = 1 . \tag{14}$$

In parametric form this becomes

$$\begin{aligned} X_R &= a \sin \omega t \\ Y_R &= b \cos \omega t \end{aligned} \tag{15}$$

and by the use of the rotation equations (7) we may write

$$\begin{aligned} X &= a \sin \omega t \cos \beta - b \cos \omega t \sin \beta \\ Y &= a \sin \omega t \sin \beta + b \cos \omega t \cos \beta . \end{aligned} \tag{16}$$

These form the parametric equations of the ellipse in the XY-plane. Rather than trying to eliminate (ωt) we shall instead assume that we may write these in the form

$$\begin{aligned} X &= E_x \sin (\omega t + \delta_1) \\ Y &= E_y \sin (\omega t + \delta_2) \end{aligned} \tag{17}$$

which we already know is true from equation (1) and our treatment in Section 2a.

Setting $X \equiv X$ and $Y \equiv Y$ in (16) and (17) and expanding (17) by trigonometry we obtain

$$\begin{aligned} E_x \sin (\omega t) \cos \delta_1 + E_x \cos (\omega t) \sin \delta_1 &\equiv a \sin (\omega t) \cos \beta - b \cos (\omega t) \sin \beta \\ E_y \sin (\omega t) \cos \delta_2 + E_y \cos (\omega t) \sin \delta_2 &\equiv a \sin (\omega t) \sin \beta + b \cos (\omega t) \cos \beta . \end{aligned} \tag{18}$$

Equating coefficients of sin (ωt) and cos (ωt) gives

$$\begin{aligned} E_x \cos \delta_1 &= a \cos \beta \\ \pm E_x \sin \delta_1 &= \mp b \sin \beta \end{aligned} \tag{19}$$

and

$$\begin{aligned} E_y \cos \delta_2 &= a \sin \beta \\ E_y \sin \delta_2 &= b \cos \beta. \end{aligned} \tag{20}$$

Eliminating δ_1, δ_2 by squaring and adding (19) and (20) gives equations for E_x and E_y in terms of a, b, and β.

$$\begin{aligned} E_x &= \sqrt{a^2 \cos^2 \beta + b^2 \sin^2 \beta} \\ E_y &= \sqrt{a^2 \sin^2 \beta + b^2 \cos^2 \beta} \end{aligned} \tag{21}$$

Next we shall multiply (19) and (20) together to obtain

$$E_x E_y \sin \delta_2 \cos \delta_1 - E_x E_y \cos \delta_2 \sin \delta_1 = a\,b \cos^2 \beta + a\,b \sin^2 \beta \tag{22}$$

which reduces to $E_x E_y \sin (\delta_2 - \delta_1) = a\,b$

or

$$E_x E_y \sin \delta = a\,b\,. \tag{23}$$

By squaring both sides of (21) and adding we immediately obtain

$$E_x^2 + E_y^2 = a^2 + b^2 \tag{24}$$

and by combining (23) with (24) we have

$$\frac{2\,a\,b}{a^2 + b^2} = \frac{2\,E_x\,E_y}{E_x^2 + E_y^2} \sin \delta. \tag{25}$$

Using equation (12) and defining

$$\tan \chi = \frac{b}{a} \tag{26}$$

(see Figure 2) we may rewrite equation (25) as

$$\sin 2\chi = \sin 2\alpha \sin \delta. \tag{27}$$

Equation (27) expresses the axial ratio as a trigonometric function of E_x, E_y, and $\sin\delta$.

3c. The Sense of Rotation

Rather than attempting to carry a sign convention throughout the preceeding analysis to explicitly indicate rotation sense we shall take a more clear-cut approach.

Referring to equations (2) and actually plotting the ellipse as a function of time will reveal the fact that rotation direction is entirely a function of δ.

Stated more definitely: $0 < \delta < \pi$ produces clockwise polarization and $\pi < \delta < 2\pi$ produces counterclockwise polarization, with the sense defined as in Section 1a. The values $\delta = 0, \pi, 2\pi \ldots$ cause the ellipse to degenerate into a straight line, i.e., linear polarization, in which case rotation is meaningless.

4. DISCUSSION OF RESULTS

4a. Summary of Equations

For the sake of clarity we shall here include Figure 2 and all associated equations of importance to evaluating the ellipse.

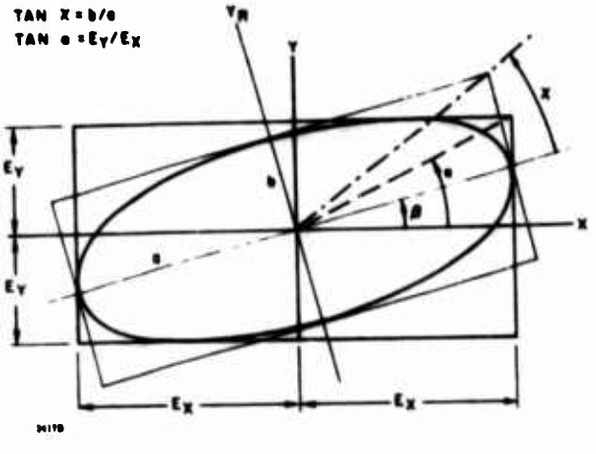

Figure 2. Definition of the Various Terms Used in This Analysis

$$\tan\alpha = \frac{E_y}{E_x} \tag{12}$$

$$\tan\chi = b/a \text{ (Axial Ratio)} \tag{26}$$

$$\tan 2\beta = \frac{2 E_x E_y \cos\delta}{E_x^2 - E_y^2} \tag{10}$$

Or, in trigonometric form,

$$\tan 2\beta = \tan(2\alpha)\cos\delta \tag{13}$$

$$\sin 2\chi = \sin(2\alpha)\sin\delta \tag{27}$$

As stated previously, no sign conventions have been followed; it is believed that confusion can be best avoided by considering the discussion in Section 4b.

4b. Limits of the Various Quantities

As already stated in Section 3c., δ as used in all equations may vary between 0 and 2π. $0 < \delta < \pi$ = C.W. rotation, $\pi < \delta < 2\pi$ = C.C.W. rotation.

From our definitions, $\tan \alpha = \frac{E_y}{E_x}$ and $\tan \chi = b/a$ are always positive numbers, where $0 \leq \alpha \leq \pi/2$ and $0 \leq \chi \leq \pi/4$.

As stated in Section 3a., β is always between 0 and $\pi/2$ and is not related to either the major or minor axis but rather to any axis of symmetry in the first quadrant. We may most conveniently relate β to the major axis by adopting a convention concerning δ.

If $-\pi/2 < \delta < \pi/2$ the major axis of the ellipse lies in the first quadrant and β may be determined directly by equation (10) or (13); note that $\cos \delta$ in this case is always positive. If $\pi/2 < \delta < \frac{3}{2}\pi$ the major axis of the ellipse lies in the second quadrant and β may be taken as 90° plus the angle calculated from (10) or (13). Cos δ is negative in this case. If $\cos \delta = 0$ we have $\beta = 0$ if $E_x > E_y$, and $\beta = \pi/2$ if $E_y > E_x$. Stated more generally: if $\tan 2\beta = 0$, $\beta = 0$ if $E_x > E_y$ and $\beta = \pi/2$ if $E_y > E_x$.

The conditions on δ may be summarized in a graphic form and are shown in Figure 3. The limits of the other variables are summarized here:

$$0 \leq \frac{E_y}{E_x} \leq \infty \qquad 0 \leq \alpha \leq \frac{\pi}{2} \qquad 0 \leq \beta^* \leq \pi$$

$$0 \leq \frac{b}{a} \leq 1 \qquad 0 \leq \chi \leq \frac{\pi}{4} \qquad 0 \leq \delta \leq 2\pi$$

$$\tan \alpha = \frac{E_y}{E_x} \qquad \tan \chi = \frac{b}{a}$$

* as defined above

4c. Specific Examples

Case I $E_y = 10$ $\delta = 90^o$

$E_x = 20$

From Figure 3 the major axis is in quadrant I and the sense is clockwise. From equation (10) tan $2\beta = 0$ and $\beta = 0$, since $E_x > E_y$ the major axis is parallel to the X axis. The ellipse is bounded by the lines X = ±20 and Y = ±10 and the axial ratio is given by equation (27) as

$$\sin 2\chi = \sin(2\alpha)(1) = \frac{2(10)(20)}{10^2 + 20^2} = \frac{4}{5},$$

therefore $2\chi = 53^o8'$, $\chi = 26^o34'$. The axial ratio is b/a = tan χ = .5000, which could have been determined by inspection in this case. The ellipse is shown in Figure 4.

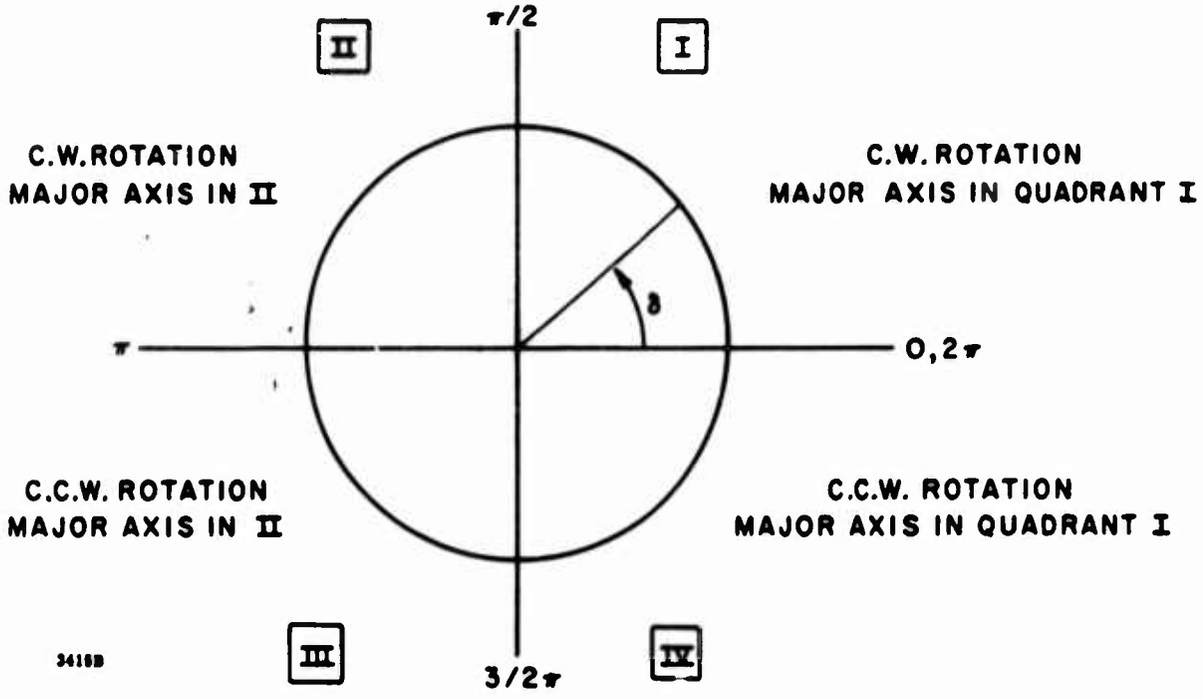

Figure 3. Sign Conventions Pertaining to δ, the Phase Angle

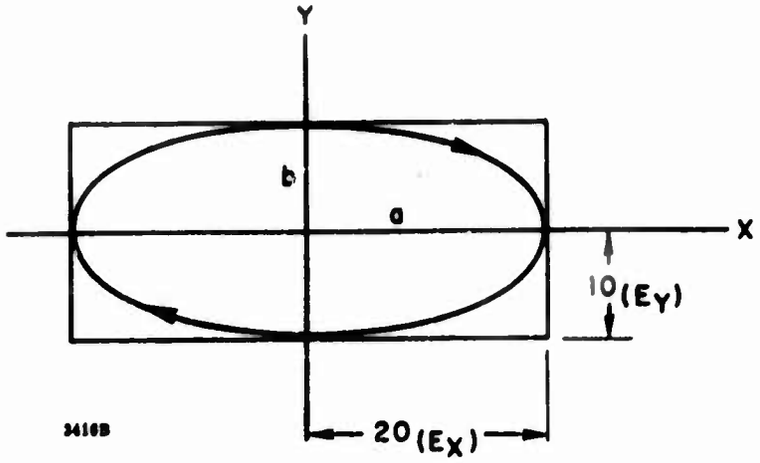

Figure 4. Illustration of Example 1

Case II $E_y = 10$ $\delta = 120^\circ$

$E_x = 20$

From Figure 3 the major axis is in quadrant II and the sense of rotation is clockwise. From equation (10) $\tan 2\beta = -\frac{2}{3}$ and $\beta = 73^\circ 9'$, or using $90^\circ + \beta$ to put us in quadrant II, $\beta = 163^\circ 10'$. Using (27) to evaluate $\sin 2\chi$ we obtain $\sin 2\chi = (\frac{4}{5}) \sin 120^\circ = 0.7008$, and $(2\chi) = 44^\circ 29'$. χ therefore is $22^\circ 14'$ and $\frac{b}{a} = \tan \chi = 0.4088$. The intercepts of the ellipse with the E_x, E_y box as given in Section 2 are $\pm (E_x, E_y \cos \delta)$ and $\pm (E_x \cos \delta, E_y)$; from this information the ellipse may be sketched and is shown in Figure 5. Note that by using Figure 3 to fix the position of the major axis, there is no confusion in determining β.

Case III $E_y = 30$ $\delta = 190^\circ$

$E_x = 26$

From Figure 3 the major axis is in quadrant II and the sense of rotation is counterclockwise. From equation (10) $\tan 2\beta = 6.82$, $2\beta = 81^\circ 40'$ and $\beta = 40^\circ 50'$. Adding 90° to this gives $\beta = 130^\circ 50'$. Equation (27) gives $\sin 2\chi = \frac{2(30)(26)\sin \delta}{(30)^2 + (26)^2}$ $= (0.99)(.1737)$ and $\sin 2\chi = .1720$. $2\chi = 9^\circ 54'$ so that $\chi = 4^\circ 57'$ and $\tan \chi = \frac{b}{a} = .0866$.

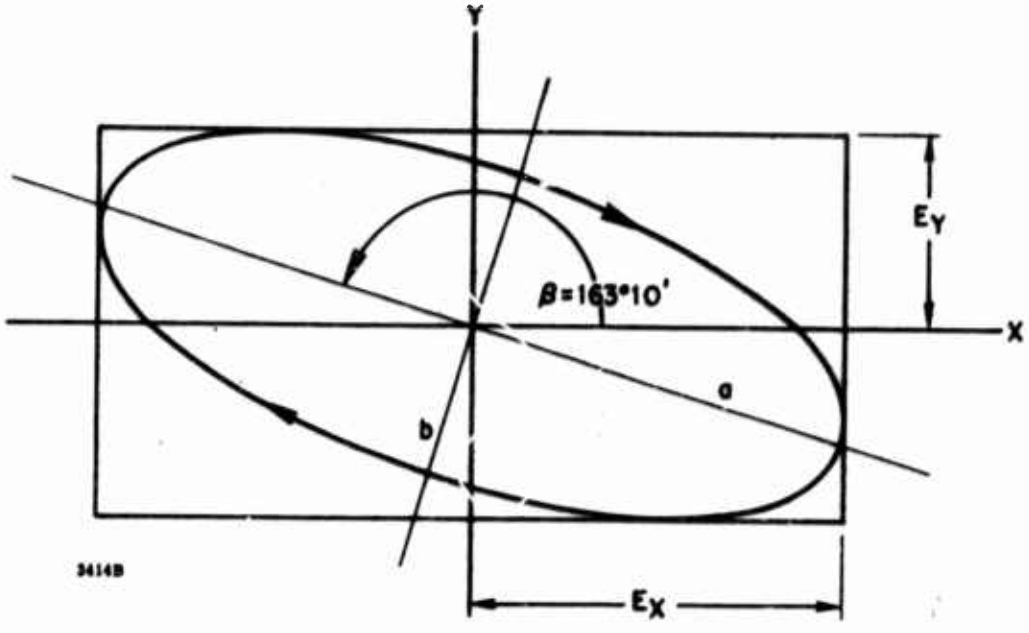

Figure 5. Illustration of Example 2

The locus of the ellipse is sketched in Figure 6; if δ had been 180° the ellipse would have degenerated into a straight line.

Several general statements about δ may prove helpful at this point.

- $\delta = 2n\pi$ $n = 0, 1, 2, \ldots$ gives a "straight line" ellipse in quadrant I
- $\delta = (2n + 1)\pi$ $n = 0, 1, 2, \ldots$ gives a "straight line" ellipse in quadrant II
- $\delta = (2n + 1)\pi/2$ $n = 0, 1, 2, \ldots$ gives an ellipse whose axes line up with the XY-axes. Note that this condition is sufficient but not necessary since if either E_x or E_y equals zero, the ellipse becomes a straight line along one axis. In this case δ has no meaning.

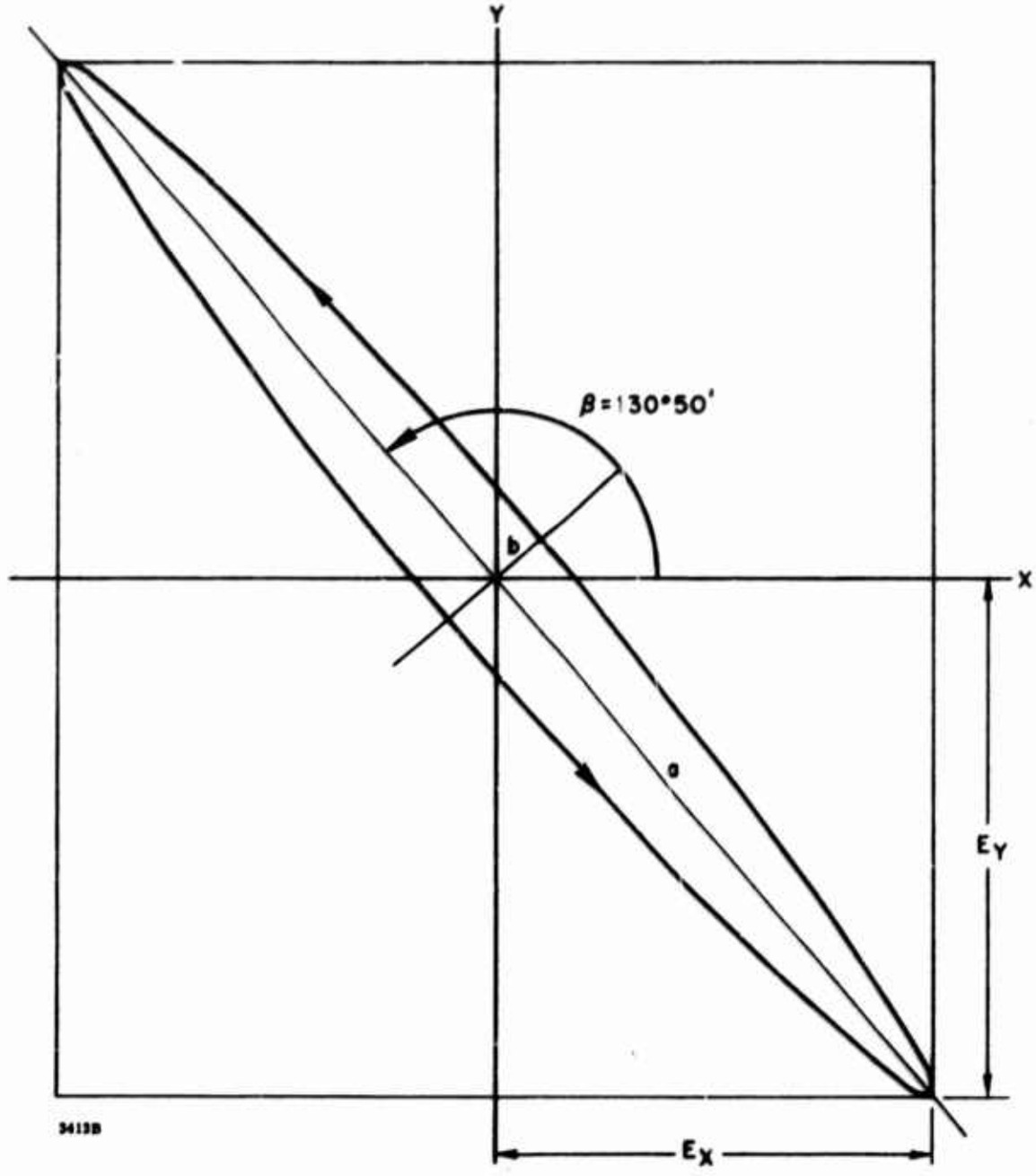

Figure 6. Illustration of Example 3

5. BIBLIOGRAPHY

1. "Reference Data for Radio Engineers," ITT, p. 666.
2. M. Born and E. Wolf, Principles of Optics, Pergamon Press 1959, pp. 24 - 35.
3. W. Shurcliff, Polarized Light, Harvard University Press 1962, Chapt. 2 (contains extensive bibliography)
4. V. Rumsey, G. Deschamps, M. Kales, J. Bohnert, "Techniques for Handling Elliptically Polarized Waves with Special Reference to Antennas," Proc. I. R. E., Vol. 39, pp. 533-552, May 1951.
5. B. Rossi, Optics, Addison-Wesley 1957, pp. 269-274.
6. J. D. Kraus, Antennas, McGraw-Hill 1953, pp. 464-486.

UNCLASSIFIED

Security Classification

DOCUMENT CONTROL DATA - R & D

(Security classification of title, body of abstract and indexing annotation must be entered when the overall report is classified)

1. ORIGINATING ACTIVITY (Corporate author)	2a. REPORT SECURITY CLASSIFICATION
Sperry Microwave Electronics Division Clearwater, Florida 33717	Unclassified
	2b. GROUP

3. REPORT TITLE

VARIABLE POLARIZER

4. DESCRIPTIVE NOTES (Type of report and inclusive dates)

Final Report December 1967 to November 1969.

5. AUTHOR(S) (First name, middle initial, last name)

L. J. Lavedan, Jr.

6. REPORT DATE	7a. TOTAL NO. OF PAGES	7b. NO. OF REFS
January 1970	73	6

8a. CONTRACT OR GRANT NO.	9a. ORIGINATOR'S REPORT NUMBER(S)
F30602-68-C-0143	
b. PROJECT NO 4506	SJ 219-5200-1
c. Task No. 450602	9b. OTHER REPORT NO(S) (Any other numbers that may be assigned this report) RADC-TR-69-432
d.	

10. DISTRIBUTION STATEMENT

This document is subject to special export controls and each transmittal to foreign governments or foreign nationals may be made only with prior approval of RADC (EMATE), GAFB, NY 13440

11. SUPPLEMENTARY NOTES	12. SPONSORING MILITARY ACTIVITY
RADC PROJECT ENGINEER Patsy A. Romanelli (EMATE) AC 315 330-4924	Rome Air Development Center (EMATE) Griffiss Air Force Base, New York 13440

13. ABSTRACT

The object of this work was to study and experimentally verify design criteria for a high power S-band variable polarizer which transforms the TE_{10} mode to vertical linear, clockwise circular, counterclockwise circular, or horizontal linear polarizations. Design objectives include switching time less than 200 microseconds, and operation at 10 MW, 20 KW average with a 40 microsecond pulse width, over the 3.1 to 3.6 GHz range. The polarizer is required to process both transmitted and receiver signals. Breadboard phasers compatible with this concept were constructed on this program and tested for limiting, breakdown level, cooling effectiveness, and magnetostrictive effects. The breadboard phasers showed no limiting up to 3 MW peak. Breakdown levels were above 3 MW peak for 2 microsecond pulse width in units without charging wires. Pressurization and the presence of hybrid mode "blips" in the transmission characteristics were found to have a significant influence on breakdown level, especially for units with charging wires.

Test results indicated that wavelength height reduction would be needed to eliminate higher order mode resonances. This would probably make it necessary to split power more than four ways to achieve full power operation.

Program objectives were reduced to avoid the prohibitive expense of constructing full scale hardware.

DD FORM 1 NOV 68 1473

UNCLASSIFIED

Security Classification

14. KEY WORDS	LINK A		LINK B		LINK C	
	ROLE	WT	ROLE	WT	ROLE	WT
Polarization						
Linear						
Circular						
Phase Shifter						
Garnet						

AFLC—Griffiss AFB NY 11 Feb 70-91